Development of the thermo-mechanical finite element model of the rotating units

Jae Woo Seo

Department of Mechanical Engineering
Graduate School of UNIST

Development of the thermo-mechanical finite element model of the rotating units

A thesis
submitted to the Graduate School of UNIST
in partial fulfillment of the
requirements for the degree of
Master of Science

Jae Woo Seo

02 . 12 . 2015.
Approved by

Major Advisor
Dr. Hyung Wook Park

Development of the thermo-mechanical finite element model of the rotating units

Jae Woo Seo

This certifies that the thesis of Jae Woo Seo is approved.

02 . 12 . 2015

Thesis Supervisor: Dr. Hyung Wook Park

Dr. Young-Bin Park

Dr. Jaeseon Lee

ABSTRACT

High-speed machining is a particularly important industrial process during which material is removed using a cutting tool with rotational and translational motion. The rotating unit is a major part of the machine tool, and is composed of a bearing, spindle, and associated surrounding components. During machining, the rotating unit is exposed to large mechanical loads, as well as significant heat generated due to friction in the bearings, which can lead to thermal deformation and failure of the spindle. To achieve reliability of the spindle system, an accurate description of the thermo-mechanical behavior of the system is useful to predict the thermal effects during the design phase.

Existing methods to simulate the thermo-mechanical behavior of rotating parts require significant computational resources because of the geometric complexity of the models. In this dissertation we discuss a finite element method (FEM) approach for calculating the thermo-mechanical behavior of the rotating unit using the commercially available software package ANSYS. We modeled the heat generated in angular contact ball bearings, and applied the heat transfer of a rotating cylinder to calculate thermal load. We explored the characteristics of the spindle system, specifically angular contact ball bearings, which are commonly used in machine tools. We carried out a geometric simplification process for angular contact ball bearings out to overcome the divergence phenomenon in the FEM simulation, which may occur because of contact between rolling elements and bearing races. We used Matrix27 elements to simulate the stiffness/damping characteristics of ball bearings, and used the ‘close gap’ function in the contact elements to implement heat transfer between the inner and outer races of the bearing. We used the thermal contact conductance to describe heat transfer between the surfaces of the bearing using the close gap function. We also determined a constant describing the thermal contact conductance for several types of bearing using a parametric simulation study, and compared the results with experimental data to determine the value of the constant. We determined the fraction of the heat flux to the inner and outer races empirically via comparisons with experimental data. Next, we carried out simulations of the rotating unit using the results of this simulation. We analyzed the thermo-mechanical behavior of the rotating unit, and compared the simulated temperature distribution and thermal deformation of the spindle tip with experimental data. We investigated three types of angular contact ball bearings, each with three different preloads. We verified the simulation results by comparing them with experimental data from a motorized rotating unit.

CONTENTS

LIST OF FIGURE

LIST OF TABLES

1. INTRODUCTION

1.1 Background

Machining is a material-removing process that has been a major component of the manufacturing industry for many years. Since the 1980s, with the development of motor and inverter technologies, belt- and gear-based spindles have been replaced with motorized spindles. It is important to overcome the productivity limits of machining processes, and high-speed machining has become increasingly popular in recent years as bearing technologies have improved. High-speed and high-precision machining is used in aerospace and automobile industries, as well as by mold and die makers.

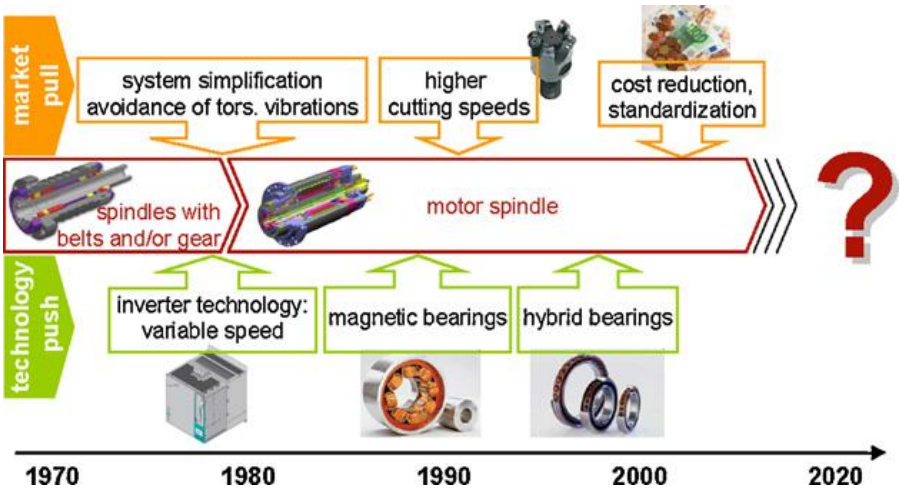

Fig. 2-1. Development of the spindle model (Abele *et al*., 2010).

High feed rates and spindle speed can negatively affect the thermal and dynamic behavior of the system. Excessive thermal load of the system can cause dynamic problems of chatter, as well as centrifugal and gyroscopic effects, which can result in sudden failure and thermal deformation. The rotating unit of the machine is composed of bearings, a spindle, a motor, housing, and surroundings. The bearings and the motor assembly are the main heat sources of high-speed rotation systems. Heat from the bearings and motor can affect the entire rotating system, which may undergo thermal deformation and cause machining errors (Krulewich, 1998). Predicting the thermo-mechanical behavior of the rotating unit is essential to ensure reliability of the system and to ensure designs are optimal. Predicting the mechanical behavior of the rotating unit requires consideration of the interactions between thermal behavior and mechanical properties under variable cutting conditions, which significantly complicates the design of the machine. The finite element method (FEM) is a popular technique for describing mechanical systems. Min *et al*. analyzed the thermal behavior of a grinding machine based on a previously developed model (Bossmanns and Tu, 1999) using ANSYS.

Other researchers have analyzed the thermal characteristics of angular contact ball bearings and simulated the temperature distribution (Min *et al*., 2007, Rai and Xirouchakis, 2008, Wang *et al*., 2013). Most researchers have used simplified models of the rotating unit because existing spindle models are not straightforward to use, and because of the complexity of the thermo-mechanical characteristics of the coupling in the bearing. Heat transfer between the inner and outer races of angular contact bearings can only be determined from an experimentally determined empirical formula that applies for specific conditions. The heat generated in the bearing is mainly caused by frictional torque due to the load, and the gyroscopic moment and frictional torque due to the viscosity of the lubricant (Harris and Kotzalas, 2007).

In this study, we modeled heat sources and simulated the mechanical behavior of the machine tool using a simplified bearing geometry. We investigated the heat transfer characteristics of the joint section of angular contact bearings. We calculated the temperature and thermal deformation of the spindle system using FEM considering the preload and the rotational speed, and verified the results experimentally.

1.2 Research objectives and approach

The goal of this study was to build an FEM model to analyze the thermo-mechanical behavior of the rotating unit. We determined the thermal characteristics of the rotating unit using existing equations, and implemented a simulation model with a simplified bearing geometry. Next, we verified the results experimentally. The main research objectives were as follows:

- To investigate the thermal characteristics of the rotating unit, including heat generation and convection under several operating conditions.
- To develop a method to describe the thermo-mechanical properties of the bearing coupling section.
- To construct a simplified FEM model to analyze the thermo-mechanical behavior of the rotating unit.

The study involved four stages:

Step 1: Determine the thermal factors affecting the rotating unit.
Step 2: Develop a bearing coupling model and carry out an experimental verification.
Step 3: Simulate the FEM model for various speeds and preload conditions of the rotating unit.
Step 4: Verify the results of the simulation by comparing the simulated temperature distribution and thermal deformation of the spindle with experimental data.

1.3 Thesis organization

Figure 1-2 presents the organization of this dissertation. Chapter 2 provides a literature review and discusses the characteristics of angular contact ball bearings, thermal factors of the rotating unit, and FEM simulations of rotating units. Chapter 3 describes the method that we applied in FEM simulations to explore the thermo-mechanical effects: a simplified bearing model considering the static thermal characteristics of the bearing. Chapter 4 describes the results of FEM simulations of the rotating unit, as well as an experimental verification. Chapter 5 provides conclusions and identifies areas for future work.

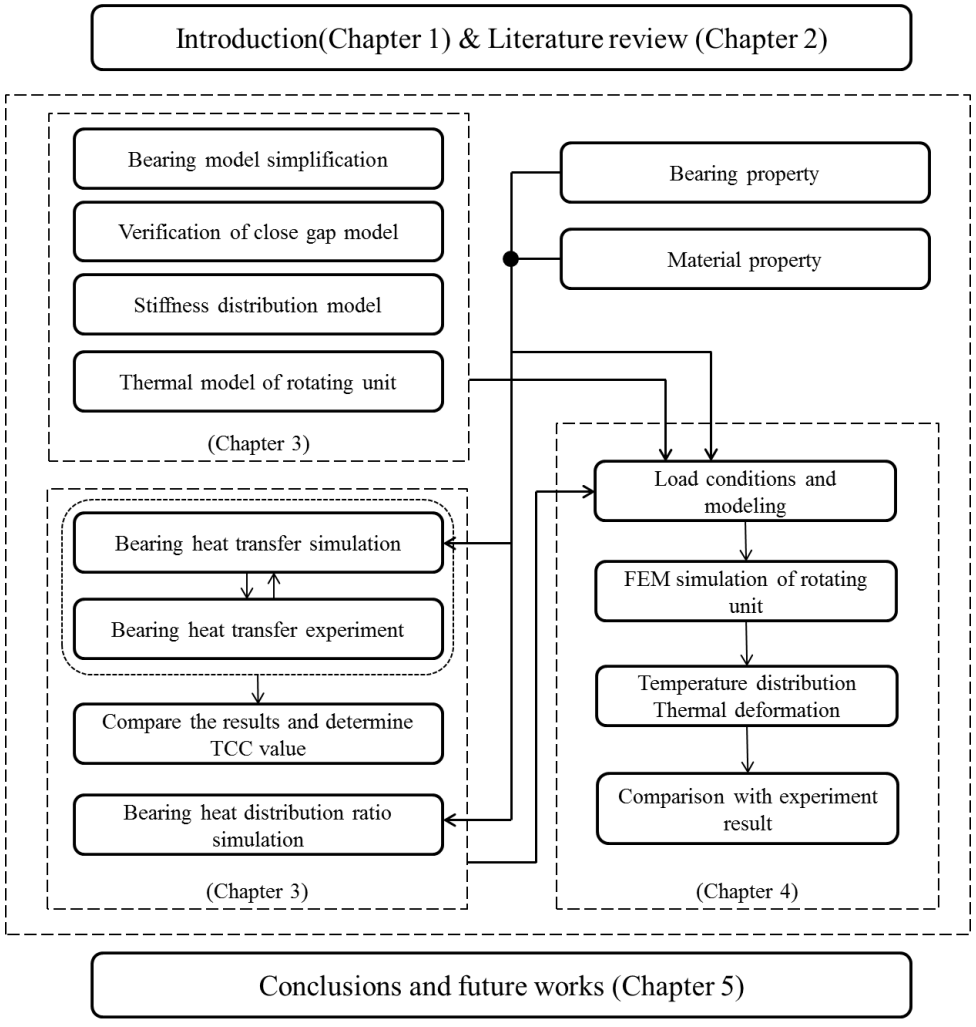

Fig. 1-2. A flow chart showing the organization of the dissertation.

2. LITERATURE REVIEW

This literature review focuses on four main components: (1) modeling of the spindle–bearing system, including dynamic, static, and thermal behavior; (2) characteristics of angular contact ball bearings, including their preload and configuration characteristics; (3) thermal factors affecting the rotating unit, including general theory of heat transfer and the tribological characteristics of bearings; and (4) FEM models for the rotating unit, including the simulation processes applied to the spindle system.

2.1 Modeling the spindle–bearing system

The spindle system is a major component of a machine tool. It should have a high stiffness, and must be highly reliable to endure severe cutting conditions with various dynamic, static, and thermal conditions, as well as various loads.

Shuzi (Shuzi, 1980) proposed a static stiffness model for the spindle to calculate the load deflection properties of the spindle system. The number and location of bearings on the spindle shaft are important factors that affect the behavior of the spindle. The dynamic properties are mainly affected by the structure of the spindle shaft, the preload of the bearings, and the stiffness of the bearings.

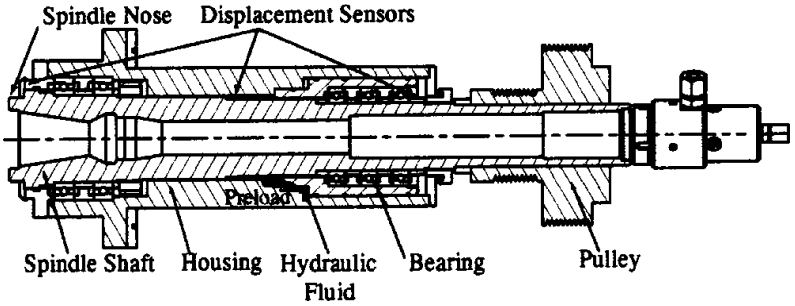

Fig. 1-1. Spindle–bearing system (Cao and Altintas, 2004).

Terman and Bollinger (Terman and Bollinger, 1965) used the finite difference method with Euler–Bernoulli beam elements to describe the dynamic properties of rotating components. Ruhl and Booker (Ruhl and Booker, 1972) proposed the first FEM model to describe the dynamic response of the rotor system, considering translational inertia and bending stiffness. Nelson (Nelson, 1980) used Timoshenko beam theory to develop a dynamic model for the rotor system using FEM, including the effects of rotational inertia, gyroscopic moments, shear deformation, and axial torque. Jorgensen and Shin (Jorgensen and Shin, 1998) proposed a spindle–bearing coupled system to describe the dynamic properties considering non-linear effects of the bearing to the cutting load, rotational speed, and total mass. They used DeMul's model to determine the bearing dynamic equations and the Timoshenko

beam theory to describe the spindle shaft.

Cao and Altintas also used the Timoshenko beam theory to model the spindle shaft and housing using FEM. They developed a dynamic model of the spindle considering the centrifugal forces and gyroscopic moments, as well as the load deflection of the angular contact ball bearing, using a nonlinear stiffness matrix, and explored the effects of speed on the natural frequencies, stiffness, contact angles, and contact forces of the bearing.

Holkup (Holkup *et al*., 2010) developed a thermo-mechanical model for a spindle with FEM using the software package ANSYS. They used this model to calculate the temperature distribution and thermal deformation caused by thermal expansion of the spindle, incorporating two-dimensional (2D) axisymmetric PLANE42 elements and CONTACT12 elements of the bearing.

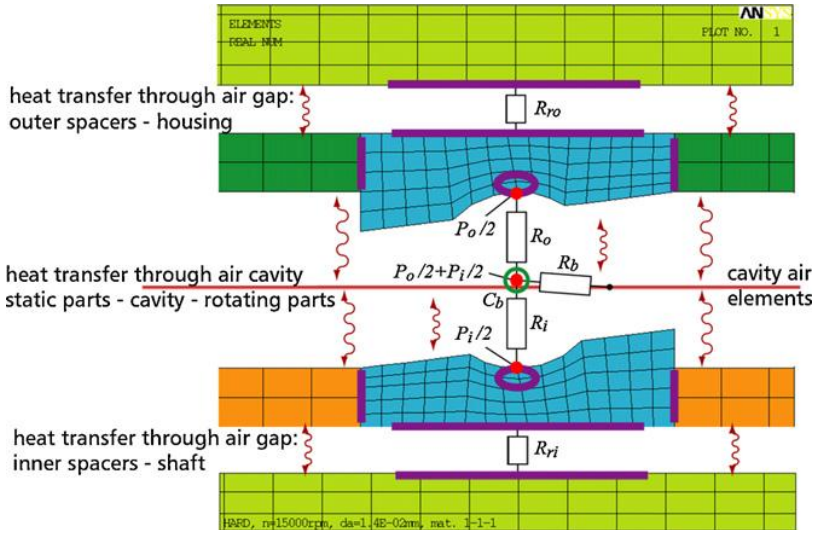

Fig. 2-2. Thermal FEM model of a bearing and surroundings (Holkup *et al*., 2010). Here, *P* is the heat generated and *R* is the thermal resistance.

Heat is generated at the interface between the inner and outer rings and the rolling elements. Figure 2-2 shows the heat generated in the bearing. Transient three-dimensional (3D) FEM models of the bearing typically include a force parameter. Researchers have described the mechanical characteristics of angular contact ball bearing using FEM; for example, Min *et al.* (Min *et al*., 2007) developed a bearing coupling analysis model using thermal contact conductance (TCC) with ANSYS.

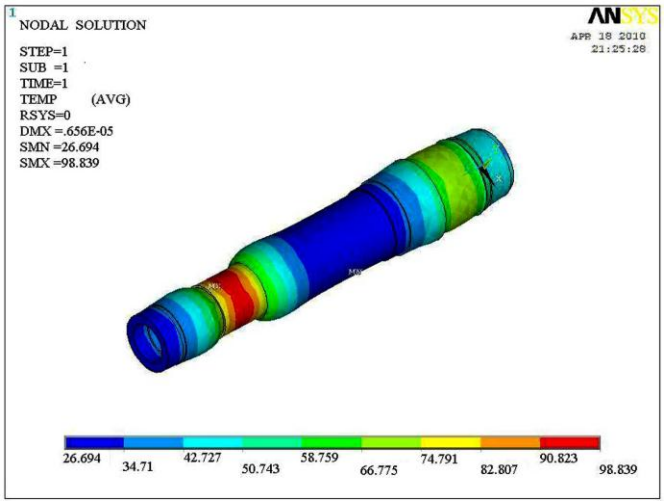

Fig. 2-3. Temperature distribution of the spindle in a CX8075 vertical milling machine (Deping Liu, 2011).

Deping Liu (Deping Liu, 2011) developed a bearing stiffness model using spring-damper elements in ANSYS, using COMBIN14 elements to describe the rolling parts of the bearing assembly, and creating a uniform circumferential geometry. This model was used to analyze the thermal, static, and modal behavior of the spindle shaft of a CX8075 vertical milling machine, as shown in Fig. 2-3.

2.2 Angular contact ball bearings

Angular contact ball bearings are the most commonly used type of bearing in machine tools due to their low friction and cost-effective maintenance (Zahedi and Movahhedy, 2012). Angular contact ball bearings are typically preloaded to provide the required stiffness, minimize vibration, and provide rotational accuracy (Alfares and Elsharkawy, 2003, Cao and Altintas, 2004).

Researchers have developed various methods of applying preload to satisfy the requirements of a wide variety of cutting conditions. Conventional methods include constant-offset preload and constant-pressure preload using a spring; more recently introduced methods include the hydraulic method, memory alloy method, and constant-offset/constant-force switching mechanism. Constant-offset preload is obtained by locking all of the races using a spacer, shim, and lock nut, and can achieve high rigidity; however, the preload increases significantly when thermal expansion occurs, which is problematic for high-speed cutting. Constant-pressure preload can be achieved using a coil spring; this is favorable for light cutting conditions where a relatively low stiffness is required.

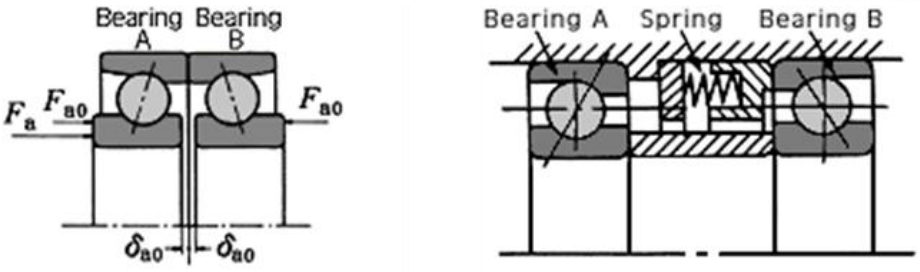

(a) (b)

Fig. 2-4. (a) Constant-offset preload and (b) constant-pressure preload.

The configuration of the angular contact ball bearing also affects the thermo-mechanical behavior of the spindle system in a manner that is not straightforward to predict. The configuration can have significant effects when thermal expansions occurs (Li and Shin, 2004a). Back-to-back and face-to-face methods can be applied with single small-angle contact ball bearings. A model to describe the dynamic thermo-mechanical behavior of such bearings is useful to achieve reliable designs of spindle systems; however, this kind of model is not straightforward because of the complex coupled effects of preload and the configuration of the angular contact ball bearing.

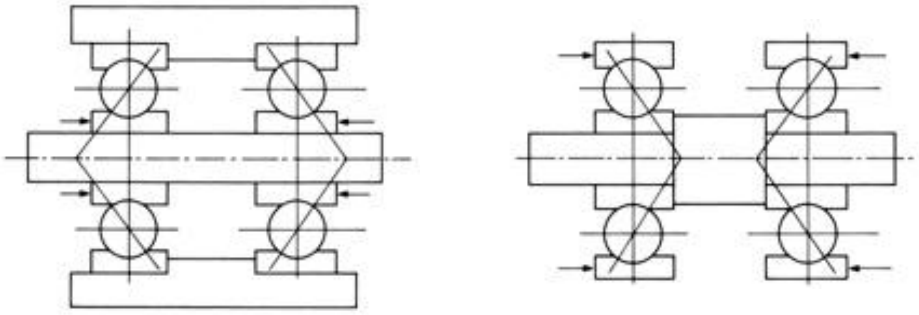

(a) (b)

Fig. 2-2. (a) Back-to-back (O) configuration and (b) face-to-face (X) configuration of a spindle system.

Chen and Chen (Chen and Chen, 2005) reported an active bearing-load monitoring and control mechanism using a load cell and piezoelectric actuators for applications in high-speed spindles. The rotation speed affects the bearing load in case of the constant-offset method. They achieved real-time adjustment of bearing preload according to the cutting conditions along with a uniform bearing load.

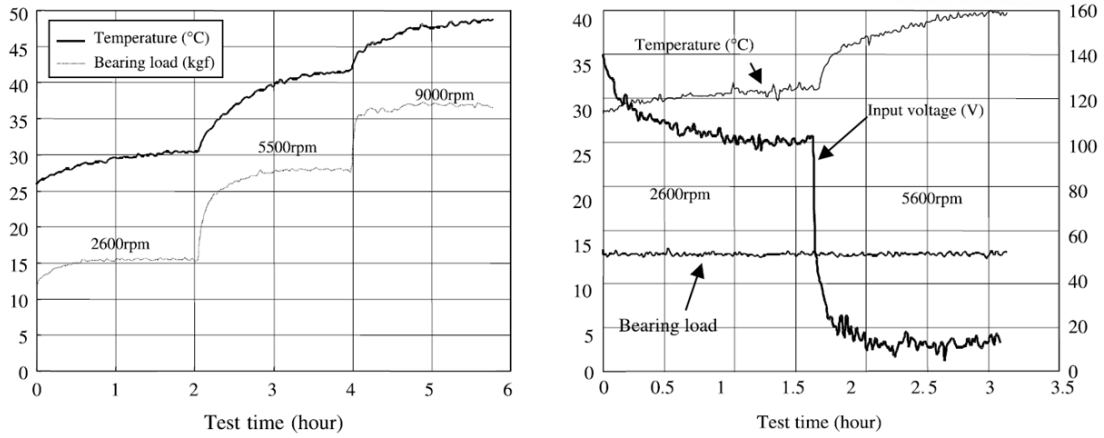

(a) (b)

Fig. 2-3. (a) Effects of spindle speed on constant-offset preload and (b) active bearing preload control (Chen and Chen, 2005).

Jiang and Mao (Jiang and Mao, 2010) developed a method for analyzing variable preload as a function of spindle rotation speed. They compared the simulated variable preload and constant-pressure preload models with experimental data. Their variable preload model exhibited reduced temperatures compared with the conventional constant-pressure model under the same cutting conditions.

2.3 Thermal effects

The major sources of heat in rotating units are the frictional forces of the bearing. In addition to the external load from the cutting face, preload affects the frictional forces on the bearing and generates heat (Holkup *et al*., 2010). The temperature of the bearing depends not only on the heat generated due to frictional forces, but also due to the following factors (Mizuta *et al*., 2003):

I. Heat generated in the bearings.
II. Thermal conductance from the inner ring to the housing.
III. Heat-transfer properties of the outer surface of the bearing housing.

Heat generated in the bearing and heat transfer to the housing can be modeled using existing heat-transfer theories, although this process is complicated when the thermal conductance of the bearing varies considerably as a function of the cutting conditions.

2.3.1 Heat generation in angular contact ball bearings

Harris and Kotzalas (Harris and Kotzalas, 2007) proposed the following expressions for the heat generated in angular contact ball bearings:

$$H_{tot} = H_0 + H_1 \tag{2-1}$$

$$H_0 = 1.05 \times 10^{-4} n M_0 \tag{2-2}$$

$$H_1 = 1.05 \times 10^{-4} n M_1 \tag{2-3}$$

where M_0 is the load torque, M_1 is the spinning frictional moment, and *n* is spindle RPM. Friction leads to load torque as follows:

$$M_1 = f_1 p_1 d_m \tag{2-4}$$

$$f_1 = 0.0013\left(P_0 / C_0\right)^{0.33} \tag{2-5}$$

$$p_1 = F_a - 0.1F_r \tag{2-6}$$

$$P_0 = X_s F_r + Y_s F_r \tag{2-7}$$

where f_1 is a factor that depends on the bearing design, p_1 is the magnitude of the load, and d_m is the mean diameter of the bearing. For angular contact ball bearings, values of X_s and Y_s depend on the contact angle, and are listed in Table 2-1 for three contact angles.

Table 2-1. Values of X_s and Y_s for three different contact angles.

Contact angle	15°	25°	40°
X_s	0.5	0.5	0.5
Y_s	0.47	0.38	0.26

The frictional torque M_0 is a function of the spindle speed, and can be described as:

$$\text{For } v \cdot n \geq 2000: M_0 = f_0 \cdot \left(v \cdot n\right)^{2/3} \cdot {d_M}^3 \cdot 10^{-7} \tag{2-8}$$

$$\text{For } v \cdot n < 2000: M_0 = f_0 \cdot 160 \cdot {d_M}^3 \cdot 10^{-7} \tag{2-9}$$

where *v* is kinematic viscosity of the lubricant and f_0 is a bearing factor for the frictional torque as a function of the spindle speed. Table 2-2 lists values of f_0 based on technical data provided by NSK.

Table 2-2. Values of bearing factor f_0 depending on the bearing type and lubrication conditions.

Angular contact ball bearings	Bearing factor f_0	
Series	Grease, with pneumatic oil	Oil bath, with recirculating oil
70..-B-72..-B	1.3	2

Zahedi and Movahhedy (Zahedi and Movahhedy, 2012) developed a thermal model of spindle systems using FEM simulations; the resulting heat generation curve is shown in Fig. 2-7 as a function of rotational speed with various preloads. The heat generated increased as a function of the rotational speed and the preload. Figure 2-8 shows the temperature of the inner and outer races of the bearing with various rotation speeds: both races had approximately the same temperature.

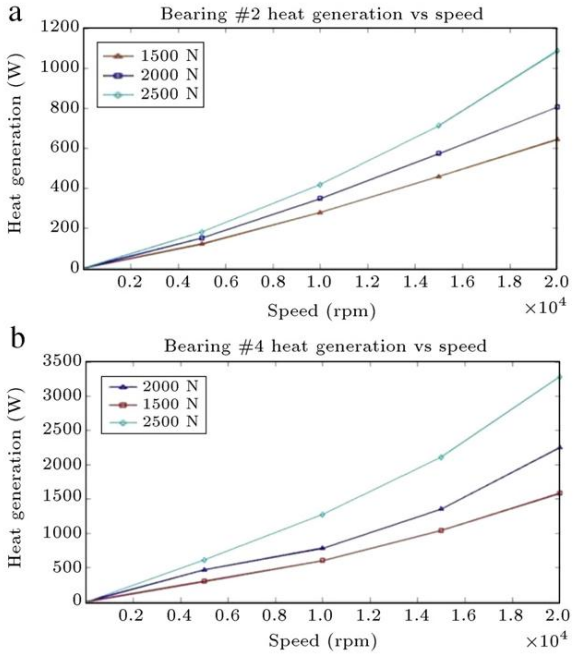

Fig. 2-4. Simulated heat generation as a function of the spindle speed for various preloads: (a) at the front bearing and (b) at the rear bearing (Zahedi and Movahhedy, 2012).

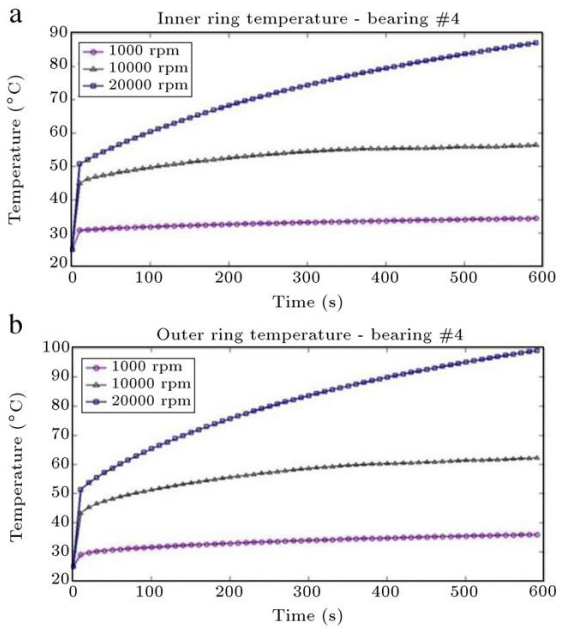

Fig. 2-5. Simulated temperature of (a) the inner ring and (b) the outer ring (Zahedi and Movahhedy, 2012).

2.3.2 Convection effects of the rotating unit

An accurate description of the cooling effects of the spindle system is not straightforward in terms of rotating conditions. The convection coefficient of a rotating spindle can be approximated as follows (Kreith et al., 2011):

$$\eta = \frac{N_u k_{air}}{d} \tag{2-10}$$

where N_u is the Nusselt number and k_{air} is the thermal conductivity of the air. The Nusselt number can be expressed as:

$$N_u = 0.133 \mathrm{Re}_d^{2/3} \mathrm{Pr}^{1/3} \tag{2-11}$$

$$\text{For, } \mathrm{Re}_d < 4.3\times10^5 \text{ and } 0.7 < \mathrm{Pr} < 670 \tag{2-12}$$

$$\mathrm{Re}_d = u_{air} d / v_{air} \tag{2-13}$$

$$\mathrm{Pr} = c_{air} u_{air} d / k_{air} \tag{2-14}$$

where Re is the Reynolds number and Pr is the Prandtl number. For a spindle speed of 1050 rpm, the heat generated in the bearing is listed in Table 4 for various preloads: the convection coefficient was calculated to be η = 85 $Wm^{-2}K^{-1}$. The fixed components of the system were assumed to have the convection coefficient of ambient air.

2.3.3 Heat transfer model for coupled components

Heat conduction of the balls is a major source of thermal resistance. A number of analytical and experimental investigations have explored the heat transfer characteristics of bearing systems. Mizuta *et al.* (Mizuta *et al*., 2003) developed a heat transfer model for angular contact bearings and compared the results of theoretical calculations with experimental data. They obtained the following approximate expression for the heat transfer rate at the interface between the balls and the bearing surfaces:

$$Q_b = 0.126\left(4.5N^{0.1} + 33\times10^{-6}N^{5/3}\right)Fa^{0.3} \tag{2-15}$$

where N is rotational speed and Fa is the preload. They focused on the heat transport properties of the balls in angular contact bearings, and explored thermal resistance of angular contact ball bearings, resulting in the following expression for the thermal conductance from the inner ring to the outer ring:

$$C_{io} = \frac{1}{R_o + R_{ob} + R_b + R_{ib} + R_i} = \frac{Q_o - Q_b}{\left(T_{i1} - T_{o1}\right) - \left(T_{i2} - T_{o2}\right)} \tag{2-16}$$

where R is the thermal resistance, T is temperature, and Q is the heat flow rate.

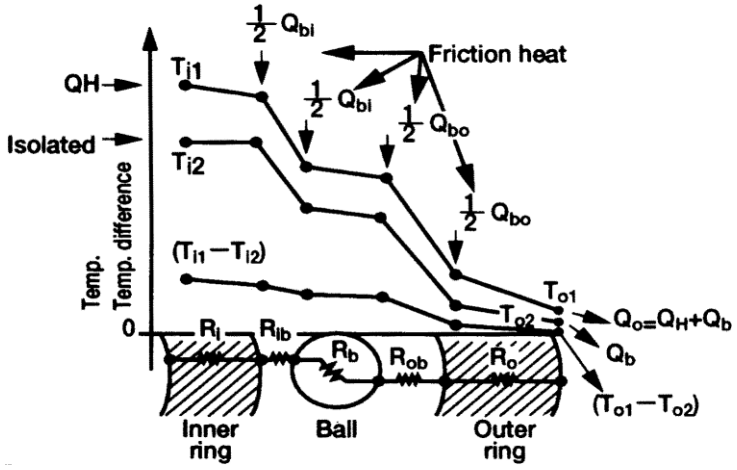

Fig. 2-9. Diagram illustrating frictional heating and thermal resistance of angular contact bearings (Mizuta *et al*., 2003).

2.4 Summary

This section discussed previous research related to general models of spindle systems. Accurate descriptions of the thermo-mechanical behavior of spindle systems are required to improve the reliability of machine tools. FEM is a particularly useful approach to analyze the thermo-mechanical

behavior of these systems. The characteristics of angular contact ball bearings depend on the configuration and the preload. Theoretical and experimental investigations have been carried out, and expressions for the heat generation at transport at bearings have been reported, as well as the convection effects of the rotating spindle.

3. THERMO-MECHANICAL MODEL OF ANGULAR CONTACT BALL BEARINGS

The bearing is one of the most important components of the spindle system, and needs to be accurately described in the design process. Angular contact ball bearings are the most common types used in machine tools, and their configuration, preload, and rotational speed affect the static, dynamic, and thermal behavior of the spindle. Models of the behavior of angular contact ball bearings are often limited to specific types of bearing, are 2D, or require excessive computational costs. In this chapter we describe a model for the thermo-mechanical properties of angular contact ball bearings using the commercially available 3D FEM software package ANSYS. The process begins with a simplification of the 3D CAD model of an angular contact ball bearing. Next, we introduce a method to incorporate stiffness and the heat generated in the bearing. We compare the experimental results and simulated data, and discuss the heat transfer characteristics of angular contact bearings.

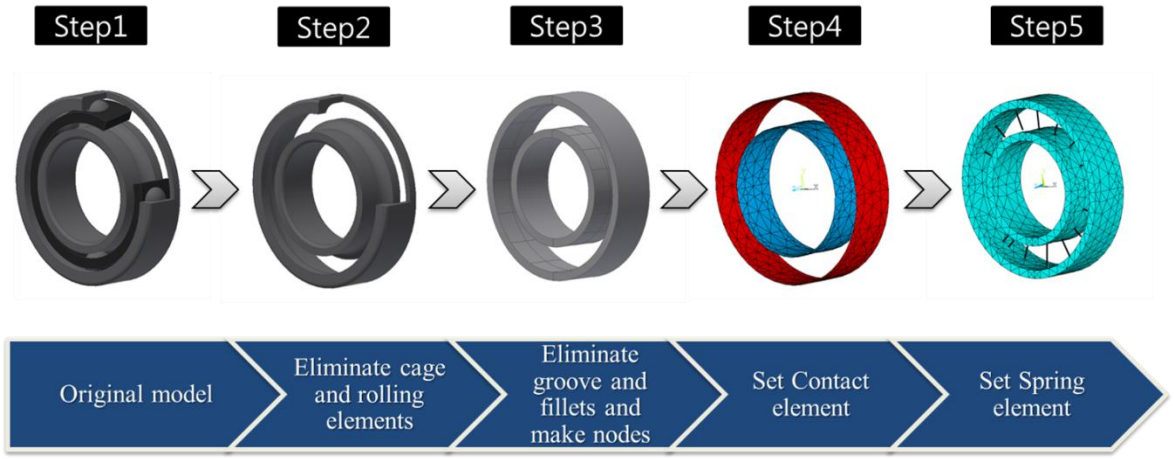

Fig. 3-1. The simplification process for the geometry of the bearings.

3.1 Simplification of bearing model

A simplified geometry is required to describe the thermal and mechanical characteristics of bearings using FEM simulations (Deping Liu, 2011). We used four steps to develop a model for the bearing. First, we eliminated the cage and rolling elements. Second, we substituted the fillets and groove geometries with plane solid parts, and used lines to describe the spring element between the inner and outer races. Third, we created 16 points on the outer surface of the inner race and the inner surface of outer race, and connected the inner and outer races of the bearings using contact and target elements. Finally, we included spring elements in the circumferential direction.

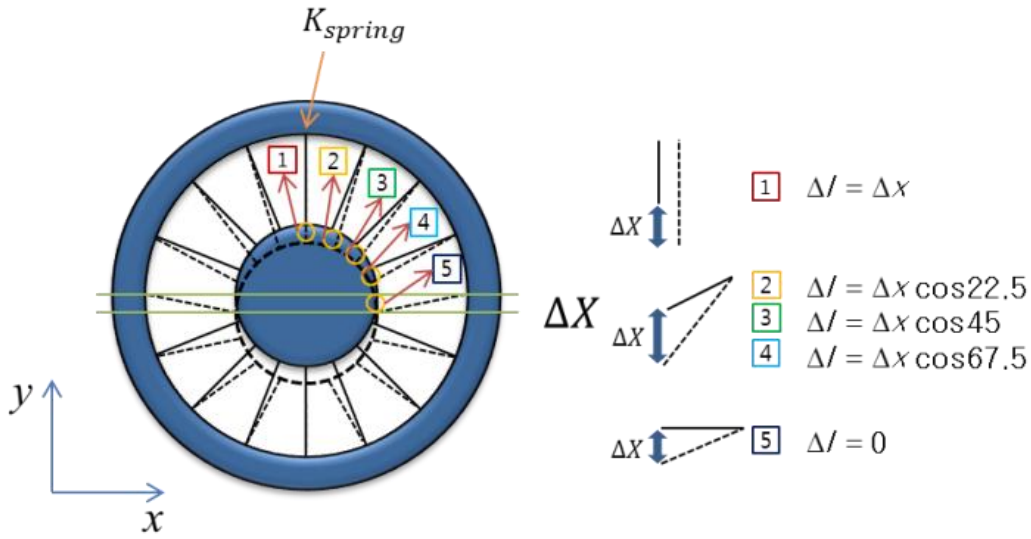

Fig. 3-2. A schematic diagram illustrating the stiffness distribution of the bearing coupling section.

3.2 Stiffness model of angular contact ball bearing

We used Matrix27 elements to describe the stiffness of coupling between the bearing and the spring elements, and assessed the stiffness in the radial and axial directions: 16 spring elements were regularly spaced by 22.5° around the ring. We assumed that the elastic energy consumed by the coupling section is equal to the sum of the elastic potential energy of the 16 spring elements. The elastic energy of each spring can be expressed as:

$$S_1 = \frac{1}{2} K_{spring} (\cos 22.5(\mathrm{i}-1)\Delta x)^2 \tag{3-1}$$

when $i = 1 \to 4$ (3-2)

where Δx is the deformation of spring and K_{spring} is the stiffness of the spring. To obtain the potential energy of the entire bearing, we double the sum of 1–4 elastic energies as follows:

$$\frac{1}{2} K_{rot} \Delta x^2 = 4 K_{spring} \Delta x^2 \tag{3-3}$$

Where:

$$K_{spring} = \frac{K_{rot}}{8} \tag{3-4}$$

and where K_{rot} is the original stiffness of the bearing. The radial stiffness can be expressed as:

$$K_{rot\_radial} = \frac{K_{spring\_radial}}{(N \times 0.5)} \tag{3-5}$$

where K_{rot_radial} is the radial stiffness of the bearing, K_{spring_radial} is radial stiffness of each spring

element, and N is the number of nodes. The axial stiffness can be expressed as:

$$K_{rot\_axial} = \frac{K_{spring\_axial}}{N} \tag{3-6}$$

where K_{rot_axial} and K_{spring_axial} are the axial stiffness of the coupling section and each of the spring elements, respectively.

For the Matrix27 elements, the stiffness should be transformed for each angle. We used the following transformation matrix to compensate for the stiffness in the X and Y directions:

$$K_{CM} = \begin{pmatrix} \cos\theta & -\sin\theta & 0 \\ \sin\theta & \cos\theta & 0 \\ 0 & 0 & 1 \end{pmatrix}^{T} \begin{pmatrix} & K_{initial} & \end{pmatrix} \begin{pmatrix} \cos\theta & -\sin\theta & 0 \\ \sin\theta & \cos\theta & 0 \\ 0 & 0 & 1 \end{pmatrix} \tag{3-7}$$

where $K_{initial}$ is the original stiffness matrix and K_{CM} is the compensated matrix.

3.3 ANSYS close gap function

The close gap function in ANSYS is a contact option that connects components. Several parameters may be controlled to implement the function, as shown in Fig. 3-3. The type of the automatic contact adjustment is changed from ‘standard’ to ‘close gap’ to use this function.

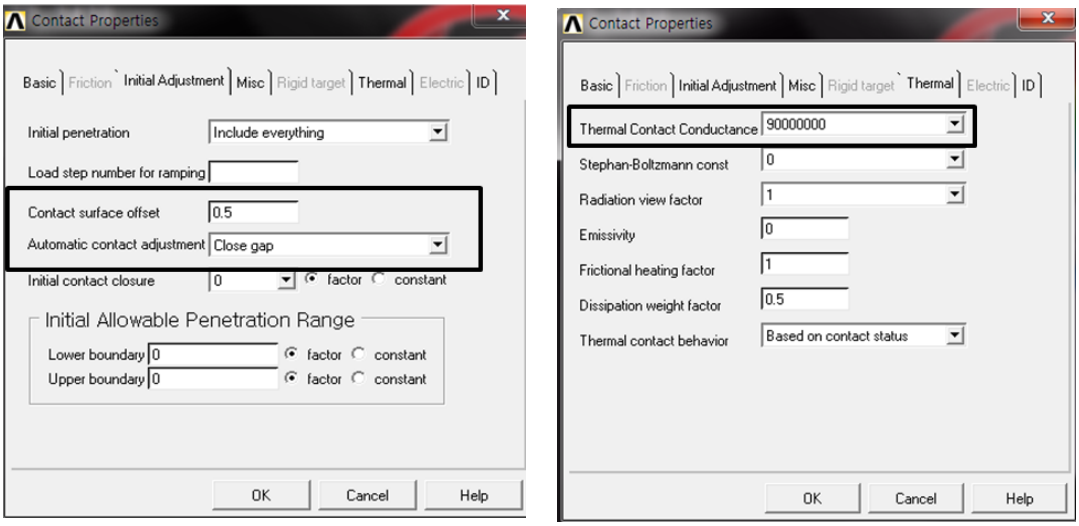

(a) (b)

Fig. 3-3. Setup for (a) the close gap function and (b) the thermal contact conductance in ANSYS.

We verified the use of the close gap function by comparing the heat transfer characteristics with those of the directly connected and simplified bearing simulation models. The connected model contains a bulk pipe between the inner and outer races, which has a specific heat capacity of zero. Those models had a small spindle shaft with no housing, as shown in Fig. 3-4.

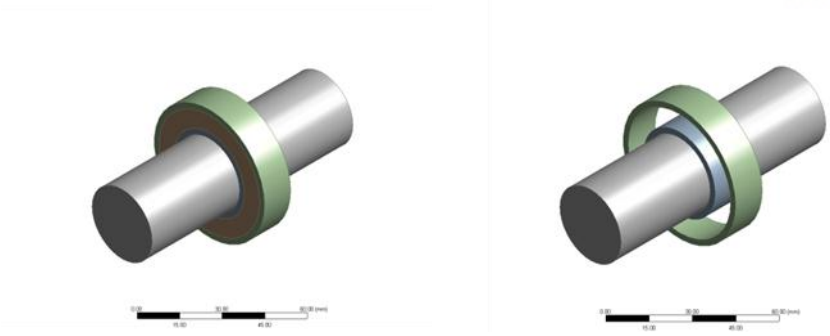

(a) (b)

Fig. 3-4. (a) 3D CAD diagram of the connected bearing model and (b) the simplified bearing geometry.

The thermal properties of the simulation models, including the thermal conductance and convection coefficient, were identical. The conditions for the simulation were heating the outer surface of outer races with a constant heat flux. Table 3-1 lists the geometric parameters of the bearings, which are shown in Fig. 3-5.

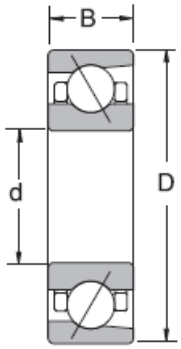

Fig. 3-5. Cross-sectional view of the angular contact ball bearing.

Table 3-1. Geometry of the bearings used in the simulation verification of the close gap option.

	Diameter of inner race [mm] *d*	Diameter of outer race [mm] *D*	Thickness [mm] *B*
Type 1	30–35	50–55	13
Type 2	30–35	50–55	26
Type 3	30–35	75–80	13

We carried out transient thermal analyses using Solid90 elements, and compared the temperature distributions of the connected and simplified bearing model among the three types of bearings. Figure

3-6 shows simulation results of the type 1 bearings; we found almost identical temperature distributions for both models. The highest temperature occurred at the outer race, and the lowest temperature at the tip point of spindle shaft. We also observed this trend in the other two bearing types, as shown in Figs. 3-7 and 3-8. The good agreement between the two models shows that the close gap function works effectively regardless of the geometry and size of the model.

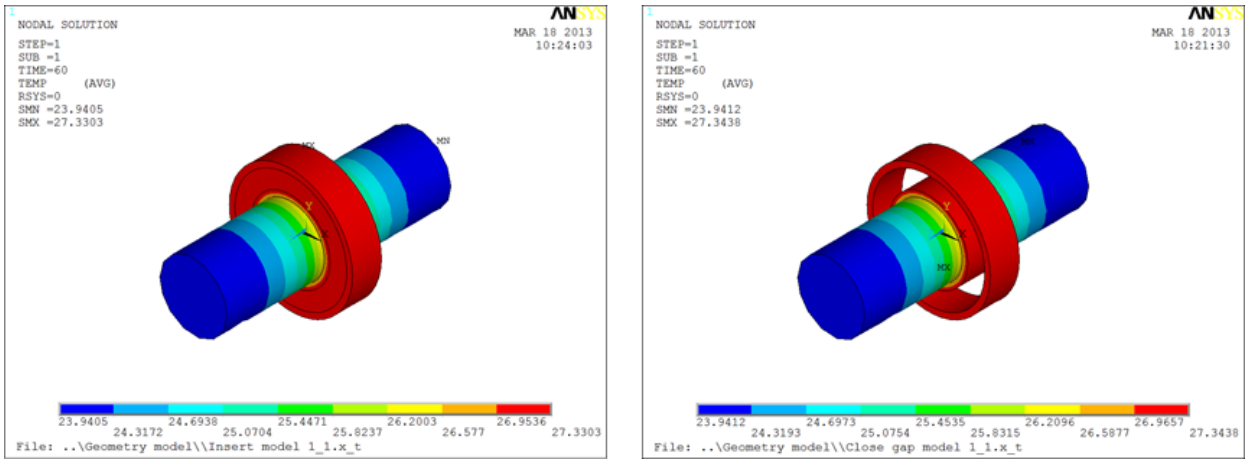

(a) (b)

Fig. 3-6. Temperature distribution for the type 1 bearings: (a) the connected model and (b) the close gap model.

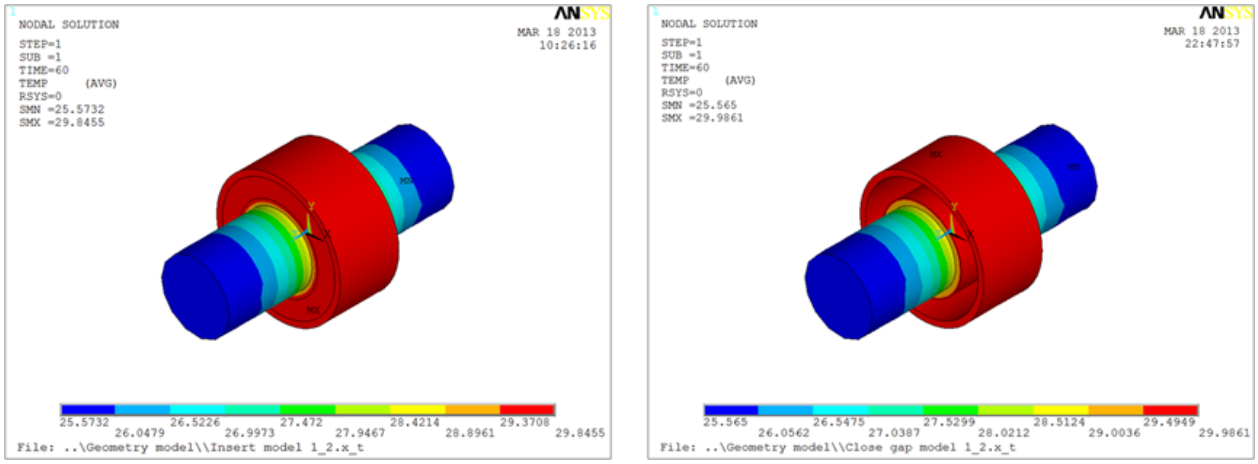

(a) (b)

Fig. 3-7. Temperature distribution for the type 2 bearings: (a) the connected model and (b) the close gap model.

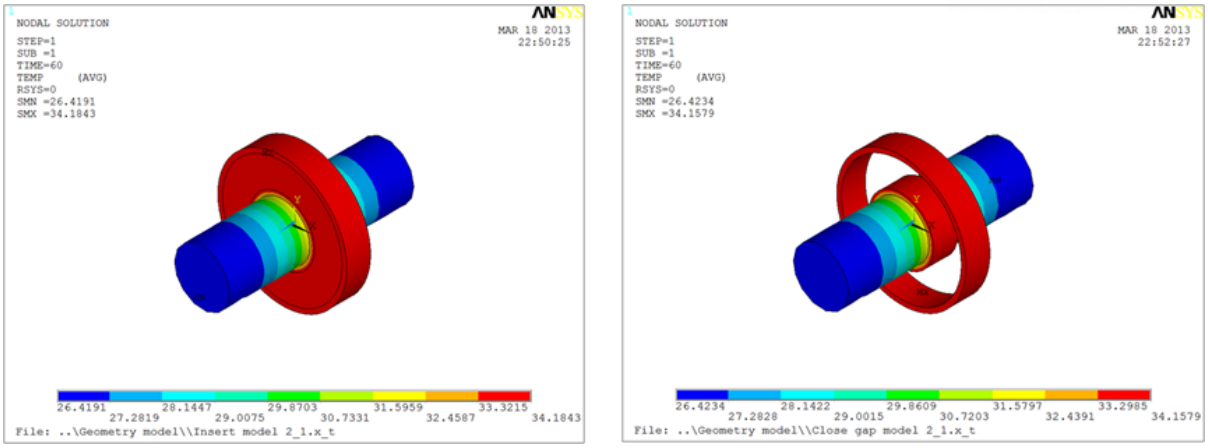

(a) (b)

Fig. 3-8. Temperature distribution for the type 3 bearings: (a) the connected model and (b) the close gap model.

We carried out simulations for two bearing models with heat fluxes of 10 W, 100 W, 1000 W, and 10000 W. The heat source was the outer surface of the outer race. Table 3-2 lists the results, which reveal that the temperature distribution was almost identical between the two models (to within ±1%). These findings verify the reliability of the close gap function for thermal analyses.

Table 3-2. The temperature distribution with the connected and the close gap models with various applied heat fluxes.

Heat flux [W]	Connected model [℃]	Close gap model [℃]
10	23.933–27.6198	23.9347–27.5889
100	41.3467–77.8909	41.3297–78.1981
1000	215.297–583.981	215.467–580.91
10000	1954.97–5641.81	1956.67–5611.1

3.4 Thermal contact conductance model for angular contact ball bearing

Describing the heat transfer characteristics of the bearing is not a straightforward process, and studies of the heat transfer characteristics of bearings have been experimental (Mizuta *et al*., 2003). Here we use the thermal contact conductance (TCC) to describe the contact between surfaces. The heat per unit area can be expressed as:

$$q = TCC \times (T_t - T_c) \tag{3-8}$$

where T_t and T_c are temperature of the two contact surfaces. The TCC can be determined approximately by comparing experimental data with the simulated spindle system, as shown in Fig. 3-9.

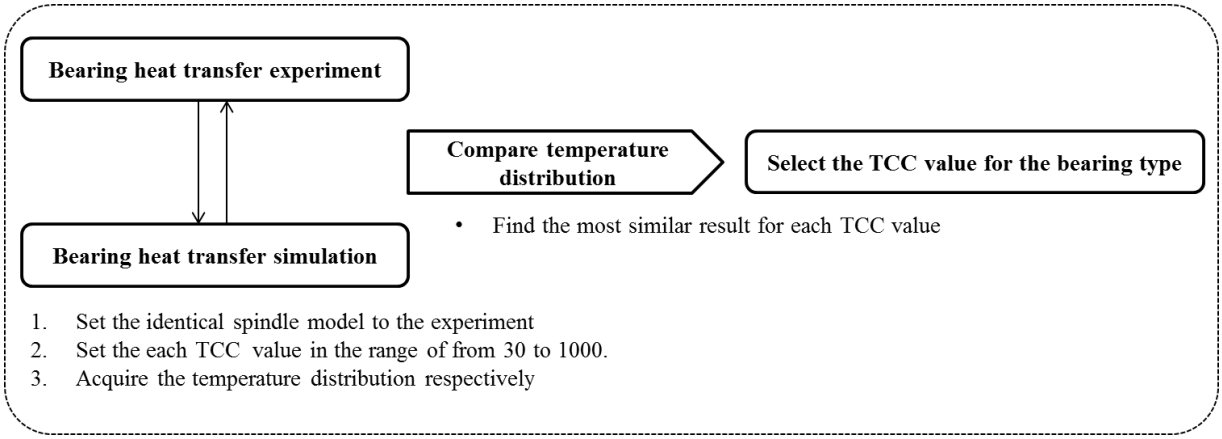

Fig. 3-9. The process used to determine the TCC for each bearing type.

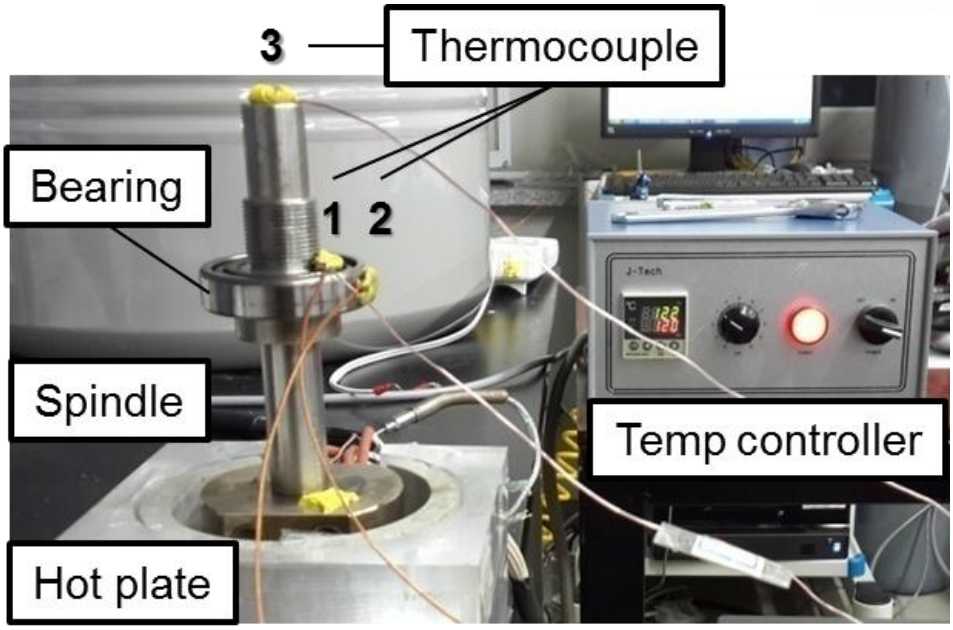

Fig. 3-10. The experimental setup used for the TCC tests.

Figure 3-10 shows the experimental setup for the TCC tests. We positioned a small spindle on a hot plate, which was used to maintain a constant temperature. We used a temperature controller to maintain a temperature of 120℃, and the surface of the plate reached a temperature of 85℃. We fixed J-type thermocouples to the ends of the spindle shaft, as well as the top surface of the inner and outer races. The tests progressed as follows:

I. Assemble the spindle with the selected bearing.
II. Position the thermocouples and fix using rubber tape.
III. Place the bearing on the hot plate and log the data for 1 hour.
IV. Cool the spindle.

We logged data using Labview with a DAQ9172 data acquisition card, and used an infrared camera to characterize the temperature distribution of the spindle during the tests, where the emissivity was 0.88. Figure 3-11 shows an image acquired using the infrared camera, with an axial view of the spindle unit equipped with the 7006C bearing. The inner race was 3℃ hotter than the outer race in the steady state, because heat was conducted from the spindle shaft, and the rolling elements behave as a thermal resistance. The cage, formed of black plastic, appeared to have a higher temperature than the other components in the infrared image; however, we attributed this to the different emissivity. Figure 3-12 shows a radial view of the spindle unit in the same environment.

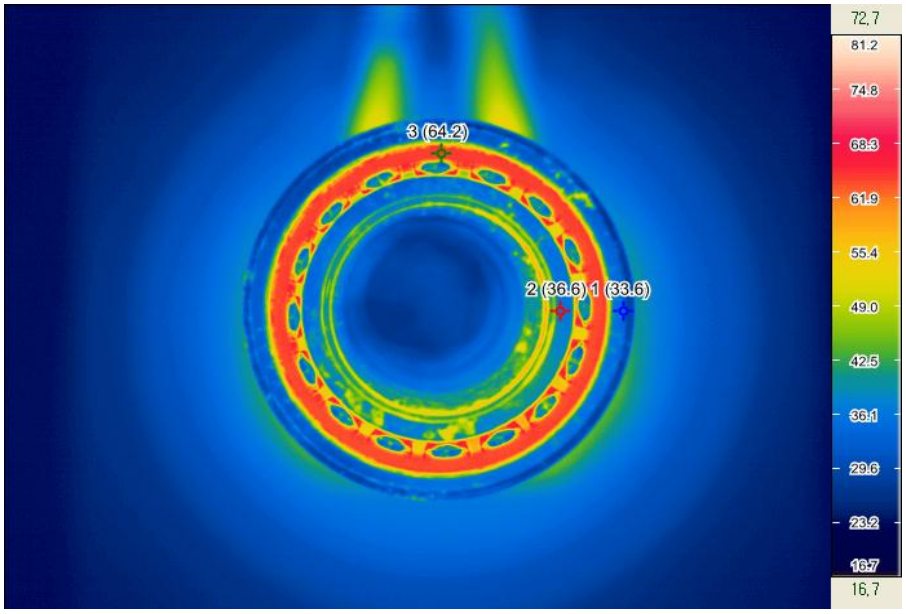

Fig. 3-11. Axial view of the spindle acquired using the infrared camera.

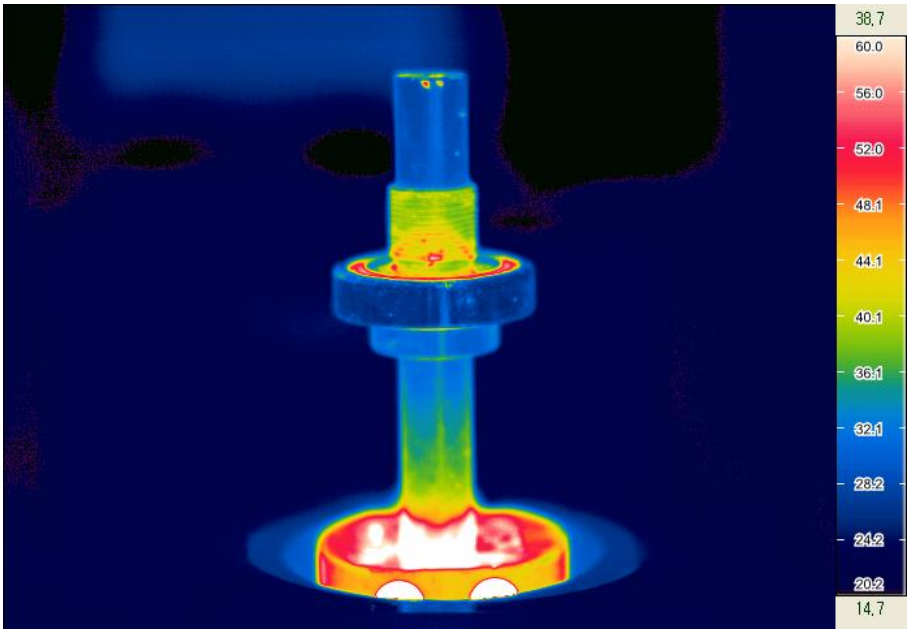

Fig. 3-12. Radial view of the spindle acquired using the infrared camera.

Figure 3-13 shows an FEM simulation of the 7006 bearing. The ambient temperature was 24℃ and the temperature of the bottom of spindle was 85℃. SOLID90 contact elements were used between the bearing races.

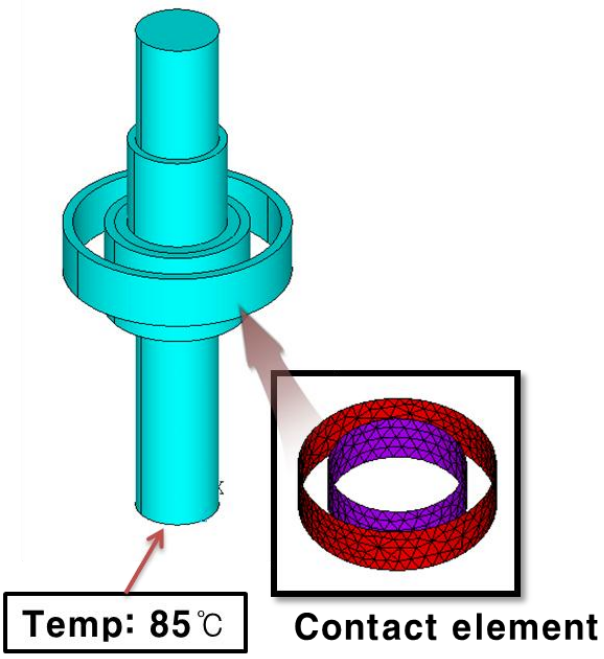

Fig. 3-13. FEM simulation of the spindle.

We systematically varied the TCC values until we achieved agreement between the results of the FEM simulation and the experiment. Figure 3-14 shows the results of FEM simulations with *TCC* = 45, Fig. 3-15 shows results when *TCC* = 90, and Fig. 3-16 shows results when *TCC* = 450. The FEM simulations show that, as *TCC* increased, the temperature difference between the bearing races become smaller.

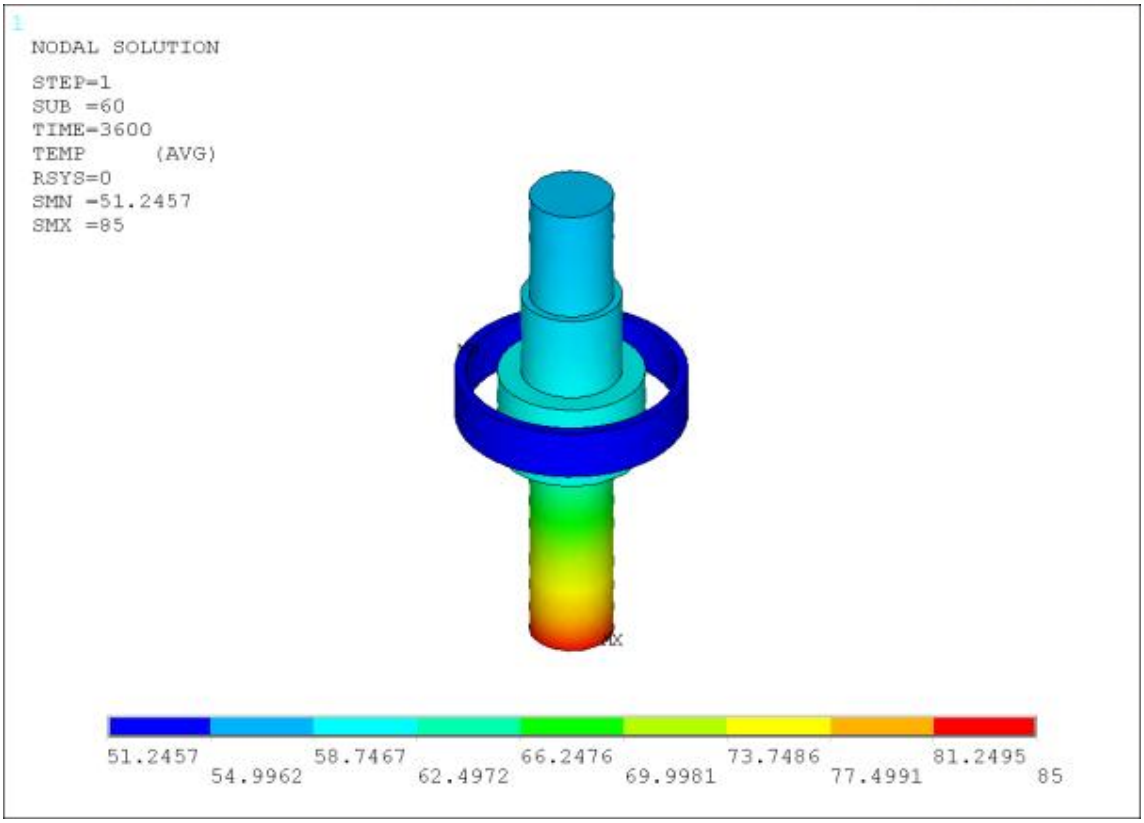

Fig. 3-14 Simulated temperature distribution of the spindle when *TCC* = 45.

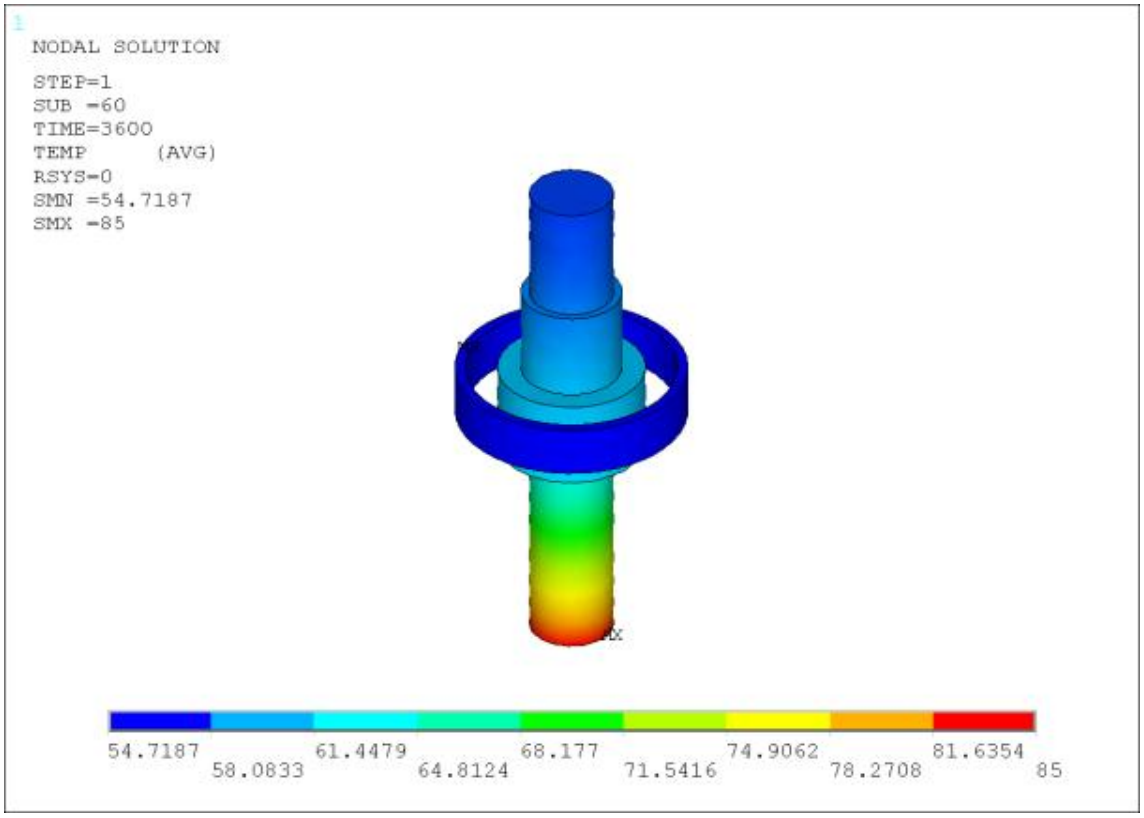

Fig. 3-15 Simulated temperature distribution of the spindle when *TCC* = 90.

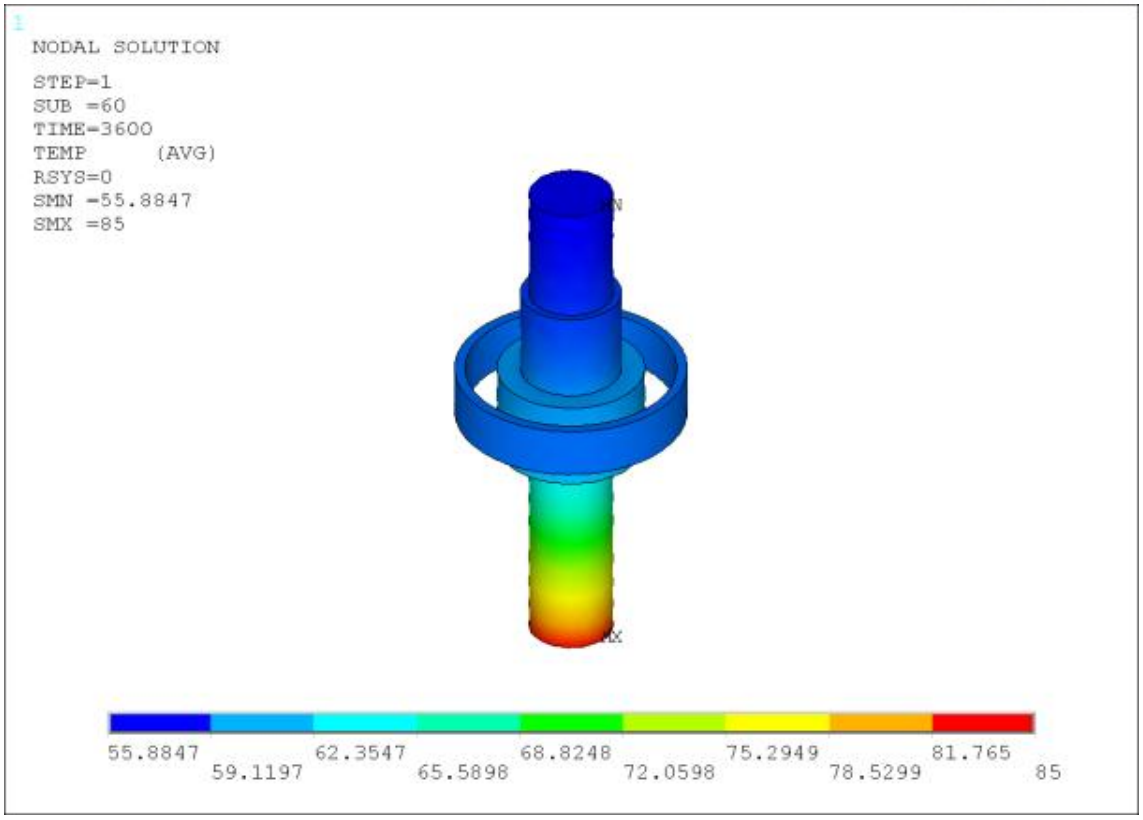

Fig. 3-16 Simulated temperature distribution of the spindle when *TCC* = 450.

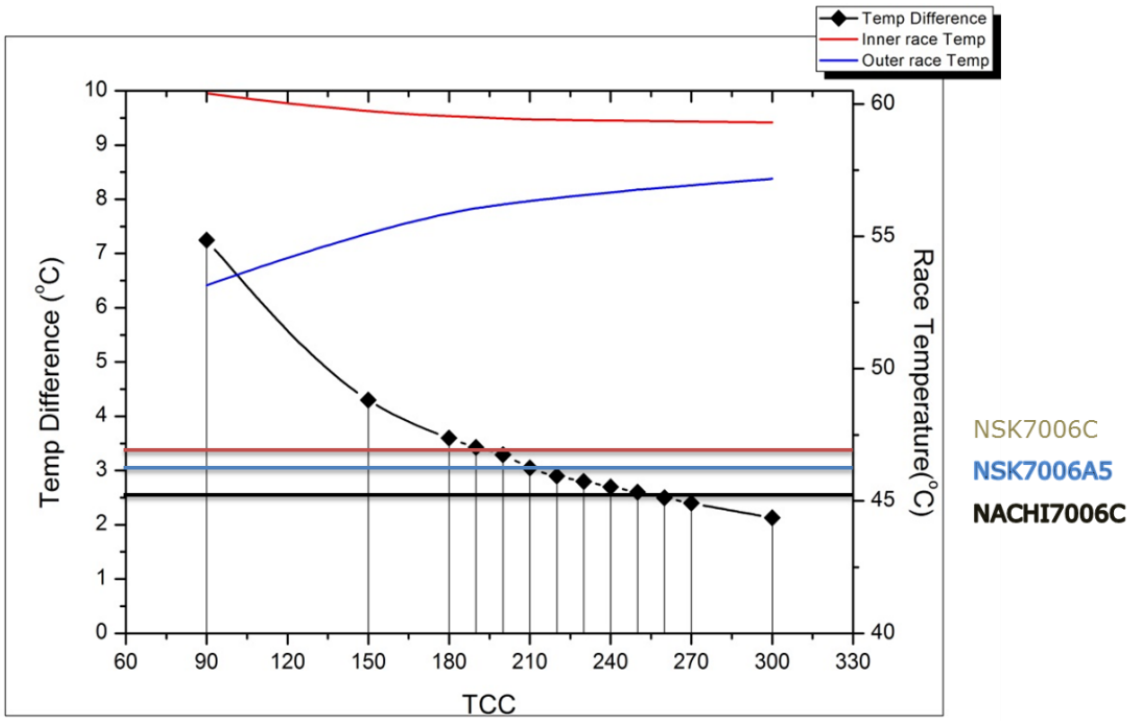

Fig. 3-17. Temperature difference between the inner and outer bearing races as a function of parameter *TCC*. Horizontal lines correspond to the experimentally measured temperature difference. The black line with the diamond symbols shows the temperature difference for each value of *TCC* used in the simulation. The red and blue lines show the simulated temperature of the bearing races.

Figure 3-17 shows the temperature difference between the inner and outer races as a function of *TCC*, which allowed us to determine appropriate values of *TCC* to obtain agreement with the experimental results. For the NSK7006C bearing, *TCC* = 190 obtained agreement between the simulated data and the experiment. Table 3-3 lists the values of *TCC* for the other 7006 series bearings.

Table 1-3. The measured temperature difference between the inner and outer bearing races and the corresponding value of TCC that obtained agreement between the simulations and the experiment.

Bearing type	Temperature difference	TCC
NSK7006C	3.36	190
NSK7006A5	3.03	210
NACHI7006C	2.53	260

We used the same procedure to determine TCC values for other types of bearing; Table 3-4 lists the results.

Table 3-4. The temperature difference and TCC values for several different types of bearing.

Bearing type	*d*	*D*	*b*	Number of balls	Mass [g]	Contact angle [°]	Ball diameter [mm]	Temperature difference [℃]
NTN7906C	30	47	9	19	58	15	5.2	2.46
NSK7006C	30	55	13	14	132	15	7.8	3.37
NSK7006A5	30	55	13	14	113	25	7.8	2.53
Nachi7006C	30	55	13	15	135	15	7.8	3.03
FAG7006B	30	55	16	14	109	40	7.8	3.00
NSK7007C	35	62	14	15	168	15	8.2	3.25
FAG7206B	30	62	16	13	197	40	9.5	3.67
NTN7206C	30	62	16	12	193	15	9.5	3.79
Nachi7206C	30	62	16	12	210	15	9.5	3.52
NSK7206A	30	62	16	13	195	25	9.5	3.68
NSK7008C	40	68	15	17	209	15	8.5	4.62
FAG7207B	35	72	17	13	282	40	11.1	4.20
FAG7306B	30	72	19	11	341	40	13	4.26
FAG7208B	40	80	18	13	367	40	11.9	4.75

Figures 3-18, 3-19, and 3-20 show the temperature difference between the inner and outer races as a function of the geometrical parameters of the bearings: size difference between the outer and inner rings, ball diameter, and outer ring diameter were used as parameters of heat transfer and exhibited similar trends. Based on the theory of thermal conductance, we would expect that the temperature difference would be greater when the separation between the races is larger; however, Fig. 3-21 shows that the contact angle had the most significant effect on the temperature difference. We investigated two different types of bearing, and found a clear relationship between the contact angle and the temperature difference.

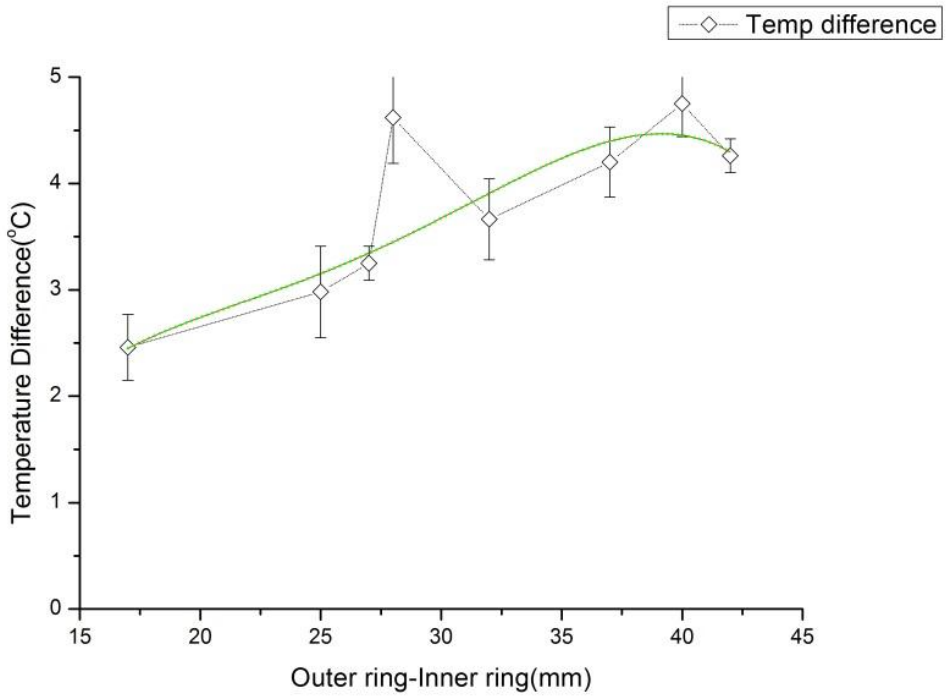

Fig. 3-18. Temperature difference between the inner and outer races as a function of the difference between the diameter of the inner and outer rings.

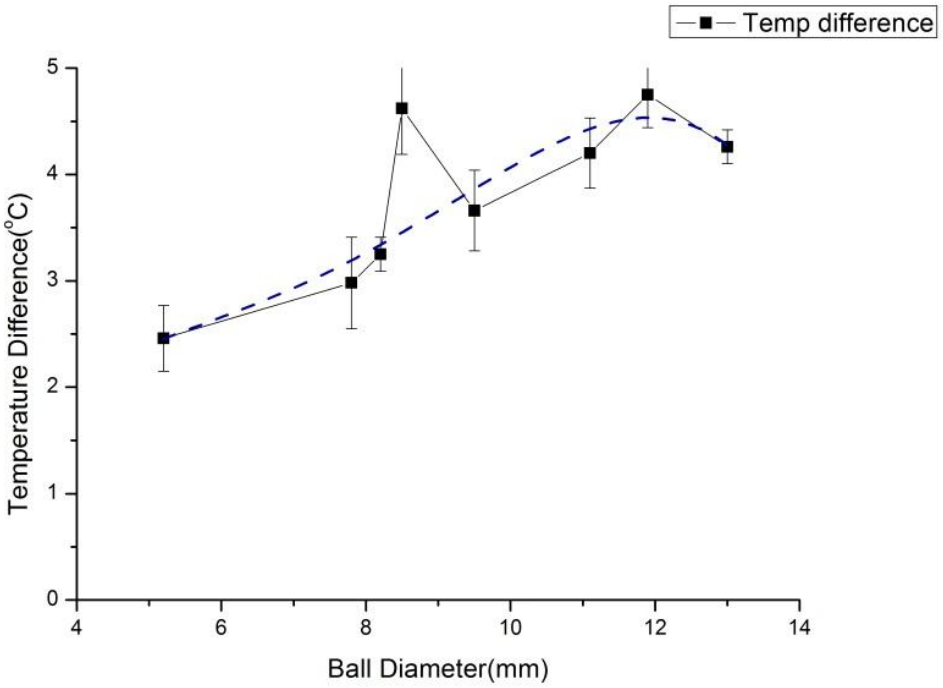

Fig. 3-19. Temperature difference between the inner and outer races as a function of the diameter of the balls.

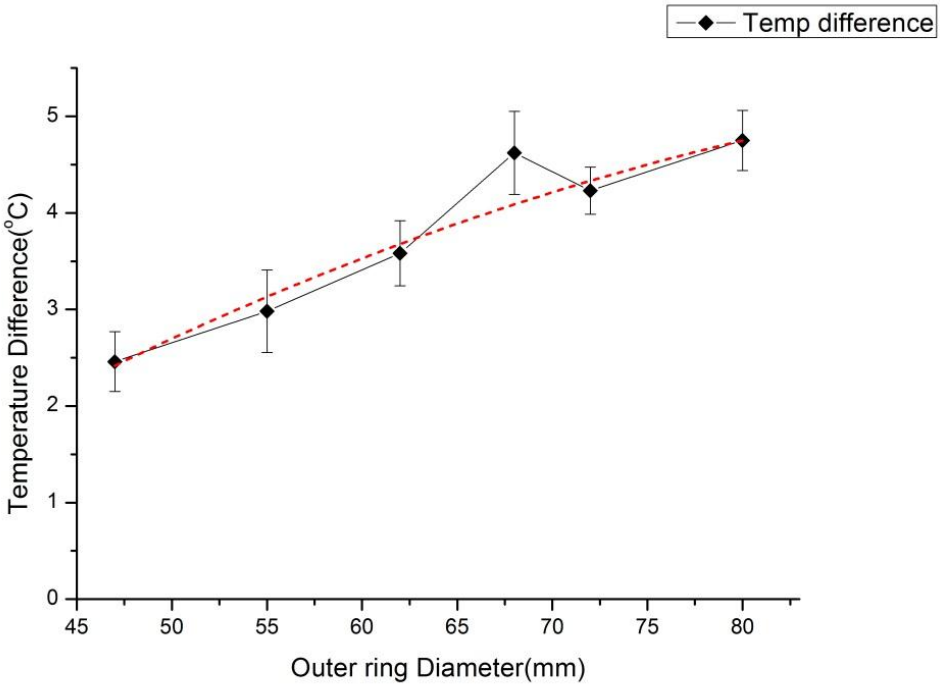

Fig. 3-20. Temperature difference between the inner and outer races as a function of the diameter of the outer ring.

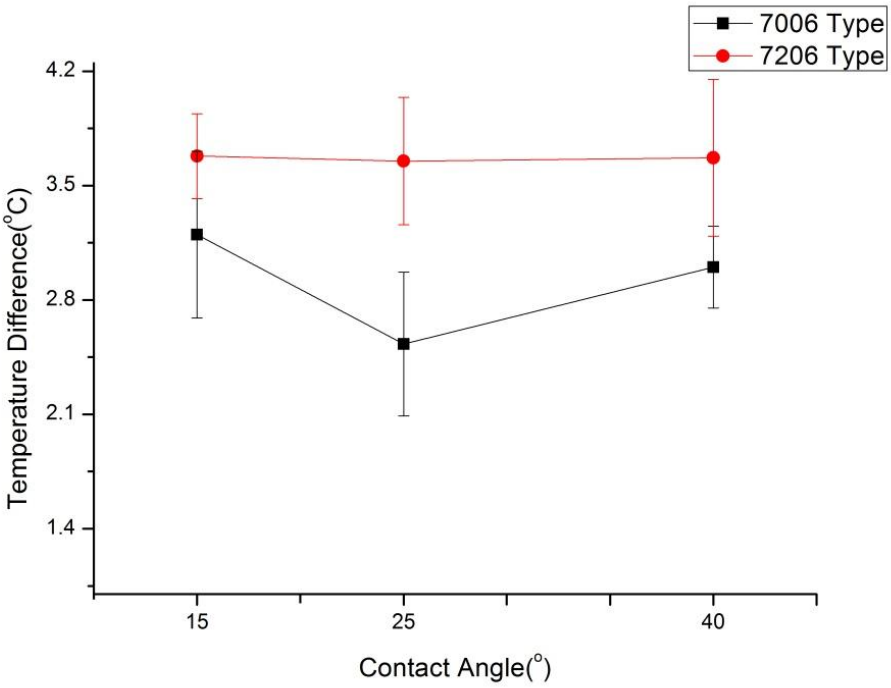

Fig. 3-21. Temperature difference between the inner and outer races as a function of the contact angle.

3.5 Heat generation distribution of the bearing races

Heat is generated in the bearings due to the frictional moment between the rolling elements and the races. Part of this heat is conducted through the rolling elements, and part through the races to the housing and spindle. The heat transfer therefore depends on the material properties of the components, as well as the heat transfer characteristics of bearings. In the simulation, heat was generated in the bearings, and conducts through the inner surface of outer race and the outer surface of inner ring. In this chapter, we discuss a method to determine the division and magnitude of heat flux and compare the simulation results with the measured temperature distribution. The TCC values of TCC for each bearing (see Table 3.4) were used in the thermal analysis of the spindle. The NSK7006C bearing was simulated using *TCC* = 190.

Table 3-5. List of simulations where the heat transported through the inner and outer races was systematically varied.

Simulation #	Inner Race [%]	Outer Race [%]
1	50	50
2	60	40
3	70	30
4	80	20
5	90	10

Figures 3-22 to 3-26 show axial views of the results of the simulations listed in Table 3-5. The temperature distributions differed depending on the fraction of the heat transported through the inner and outer races. Zahedi and Movahhedy found that inner and outer races had similar temperatures (see Fig. 2-8). We found that simulated temperature differences with 70% of the heat conducted through the inner race and 30% through the outer race resulted in equal temperature of the two races. Table 3-6 lists the simulation parameters that provided agreement with the experimentally observed temperature distributions.

Table 3-6. The heat distribution fraction and TCC for each bearing type.

Bearing type	Heat distribution fraction	TCC
NSK7006C	Inner 70%; outer 30%	190
NSK7006A5	Inner 70%; outer 30%	210
NACHI7006C	Inner 80%; outer 20%	260

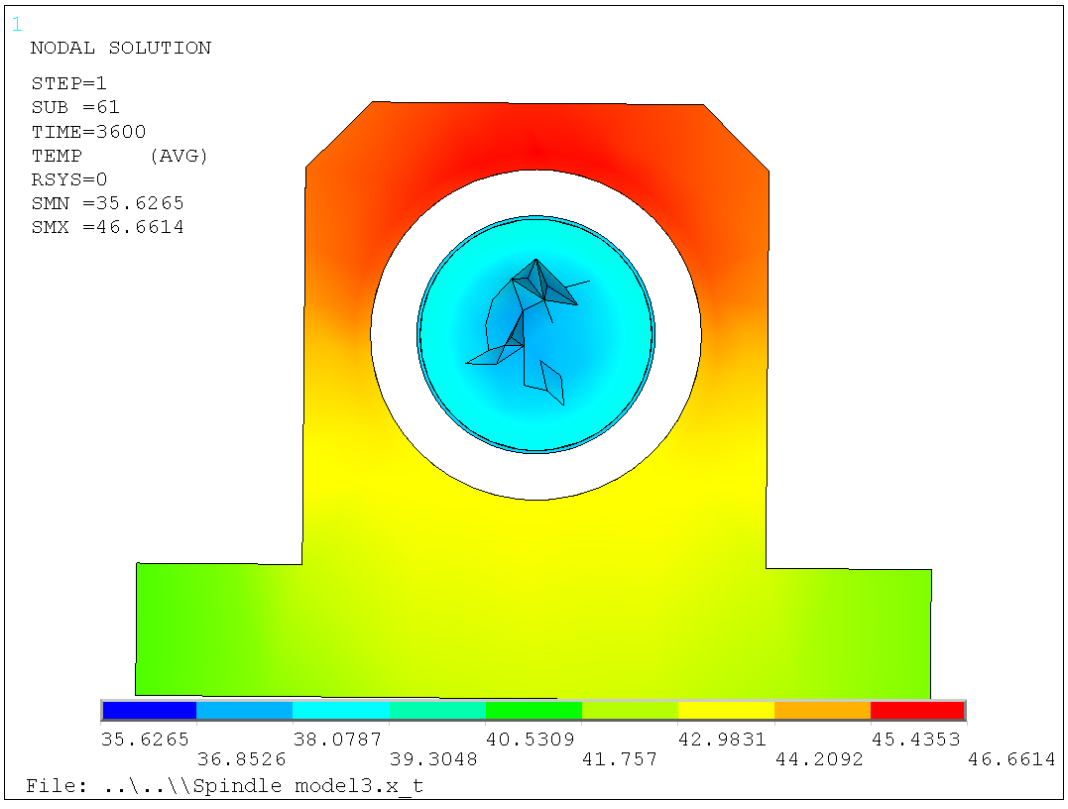

Fig. 3-22. Temperature distribution for simulation #1.

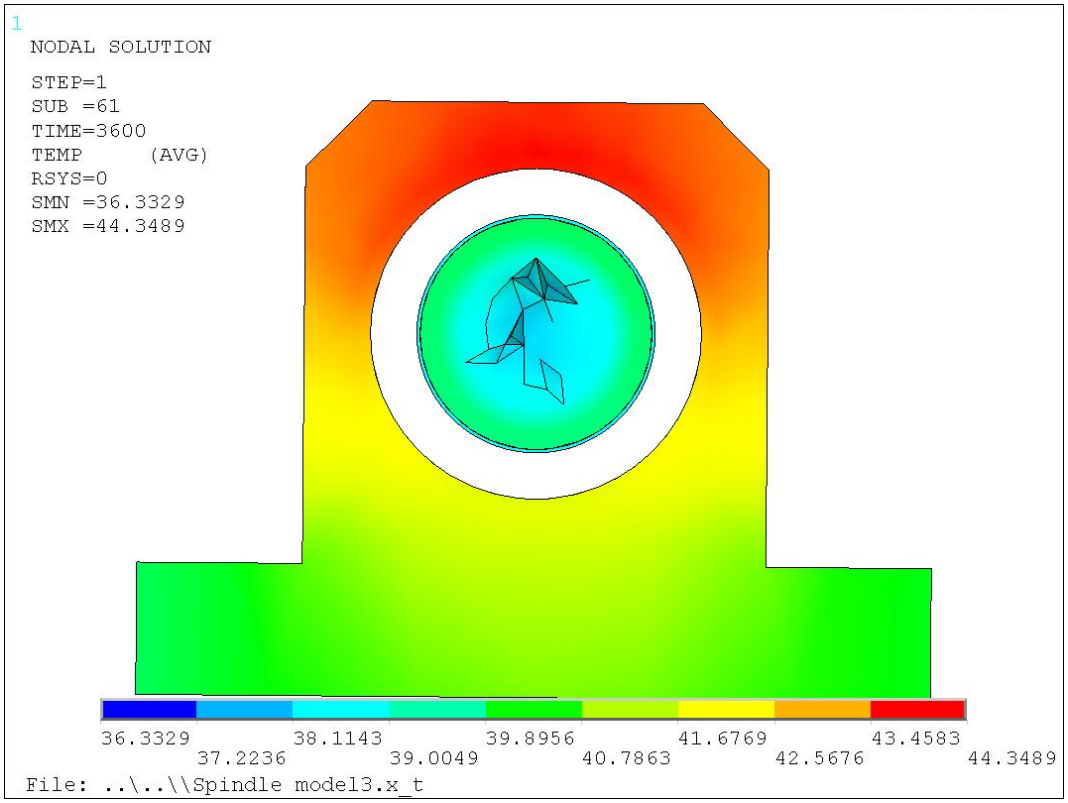

Fig. 3-23. Temperature distribution for simulation #2.

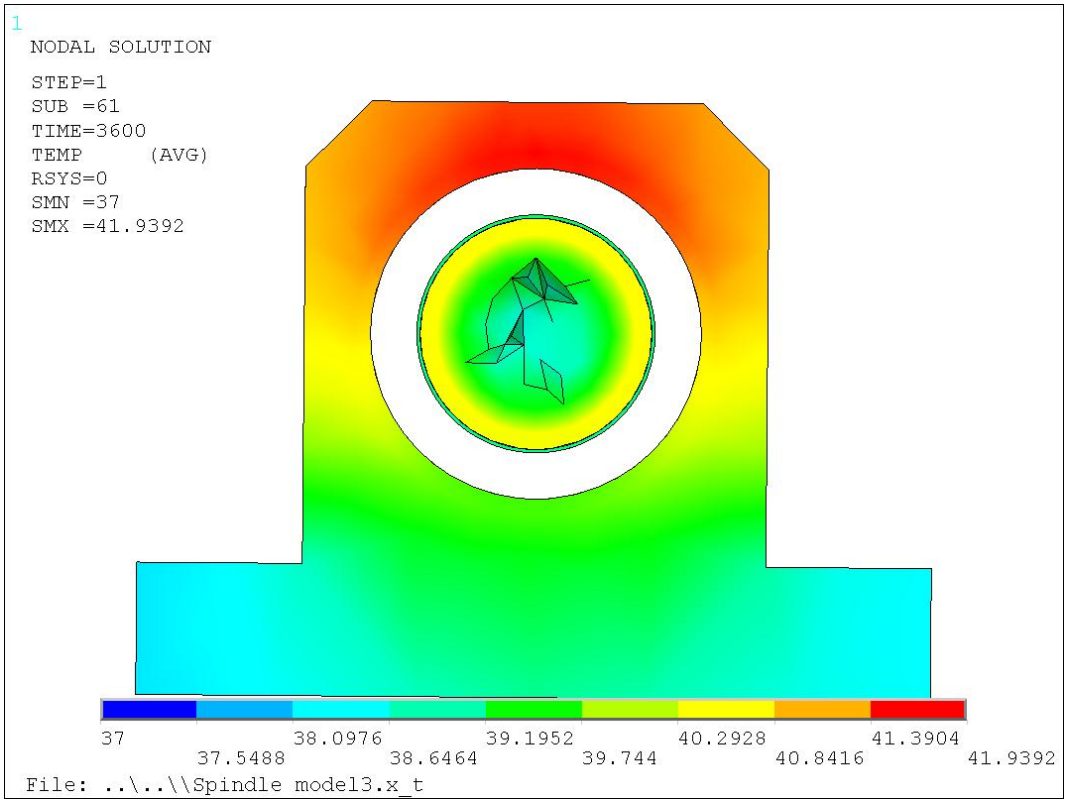

Fig. 3-24. Temperature distribution for simulation #3.

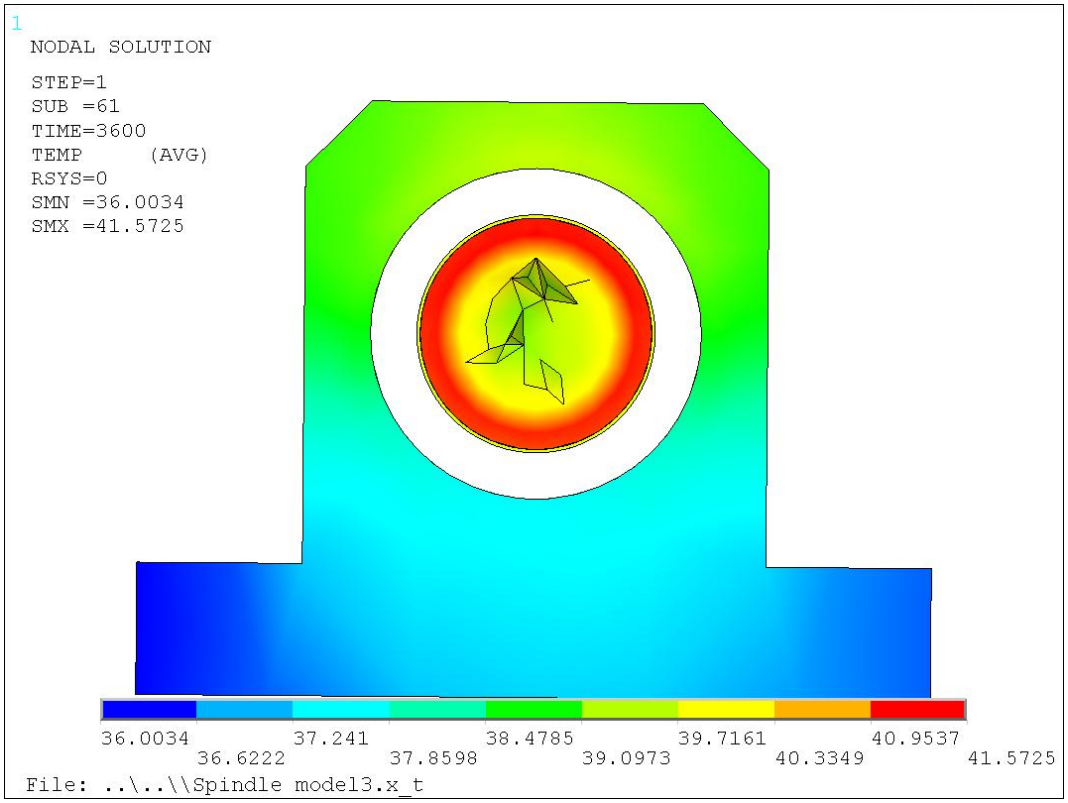

Fig. 3-25. Temperature distribution for simulation #4.

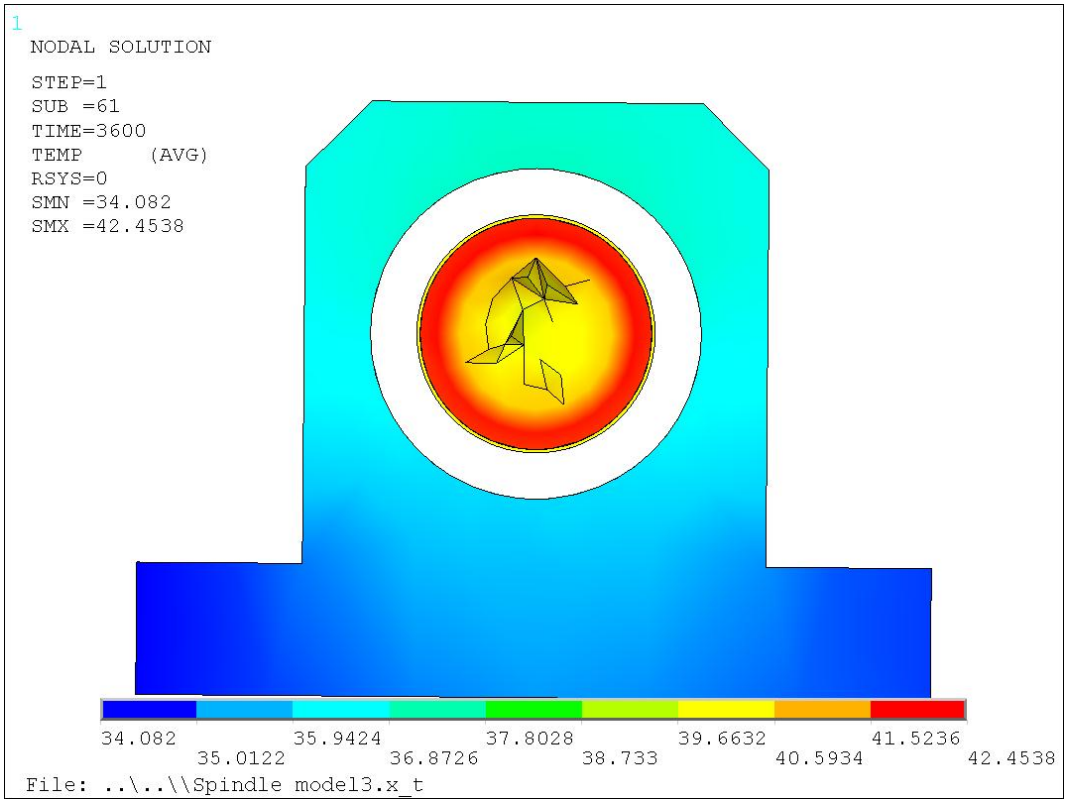

Fig. 3-26. Temperature distribution for simulation #5.

3.6 Summary

In this chapter, we described FEM simulations of the steady-state thermal characteristics of angular contact ball bearings. We simplified the bearing model to facilitate the FEM simulations, and introduced a stiffness distribution method using the spring element available in ANSYS. We used the ANSYS contact function to describe the thermal characteristics of the angular contact bearings, connected the bearing races using the close gap function, and used a systematic approach to determine TCC values for each type of bearing based on comparisons with experimental data. We simulated the heat generated in the bearing by applying a heat flux to the surfaces of bearing races, and conducted simulations to determine the distribution of this heat flux in order to ensure agreement with experimentally measured data.

4. FEM MODEL OF THE ROTATING UNIT AND EXPERIMENTAL VERIFICATION

In this chapter, we discuss an FEM model of a rotating unit, including the load conditions, and an experimental verification of simulated data. We discussed the load conditions of the simulation in chapter 3. This chapter describes FEM simulation using ANSYS Classic, along with the simulated thermal deformation and temperature distributions. For the experimental verification, we measured thermal deformation using a capacitive sensor, and measured temperature using thermocouples. We investigated three types of bearing, each with three different preloads.

4.1 FEM model of rotating units

The FEM model described in this chapter uses a coupled analysis, which complicates the simulation process. Figure 4-1 shows an overview of the simulation. We used a 3D CAD model of a rotating unit, which was developed using Autodesk Inventor 2013. We imported the CAD file into ANSYS, and converted it to a solid model, as shown in Fig. 4-2. We used the solid model for both the thermal and static analysis, beginning with the thermal analysis of the system. We sued SOLID87 elements, with 10 nodes for each degree of freedom of temperature. Specifically, we used the material properties of steel and aluminum, and meshed the model using the automatic option. We used the contact elements TARGE170 at the inner surfaces of outer race, and CONTA174 elements at the outer surfaces of inner race. We used TARGE170 and CONTA174 elements to describe surface-to-surface contact with 3D 8-node elements. We made adjustments using the close gap function, and used the TCC values for the bearings described in chapter 3. The load conditions for the thermal analysis included an ambient reference temperature of 24℃, and we applied the heat flux as described in section 2.3.1. The transient analysis was over a period of 1 hour, during which we assessed load step and temperature per node.

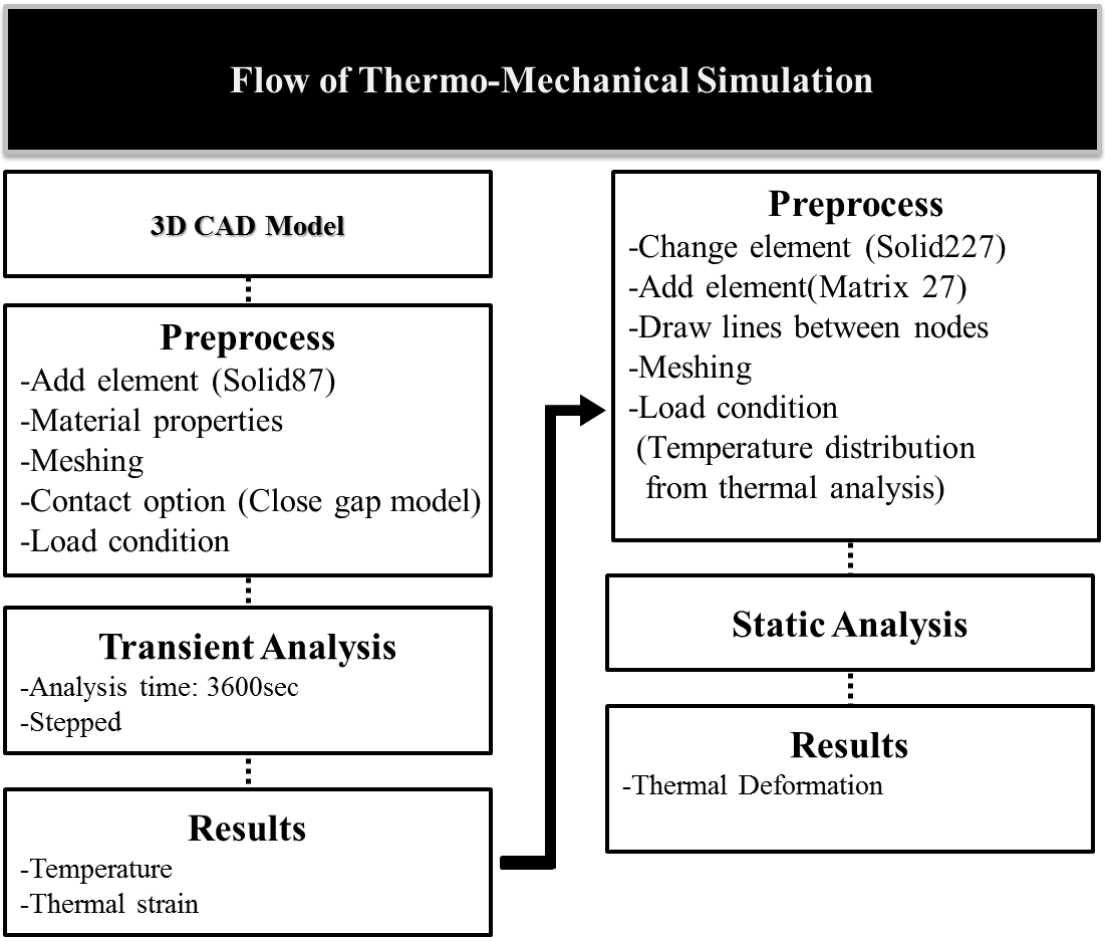

Fig. 4-1. Flow chart showing the thermo-mechanical simulation process.

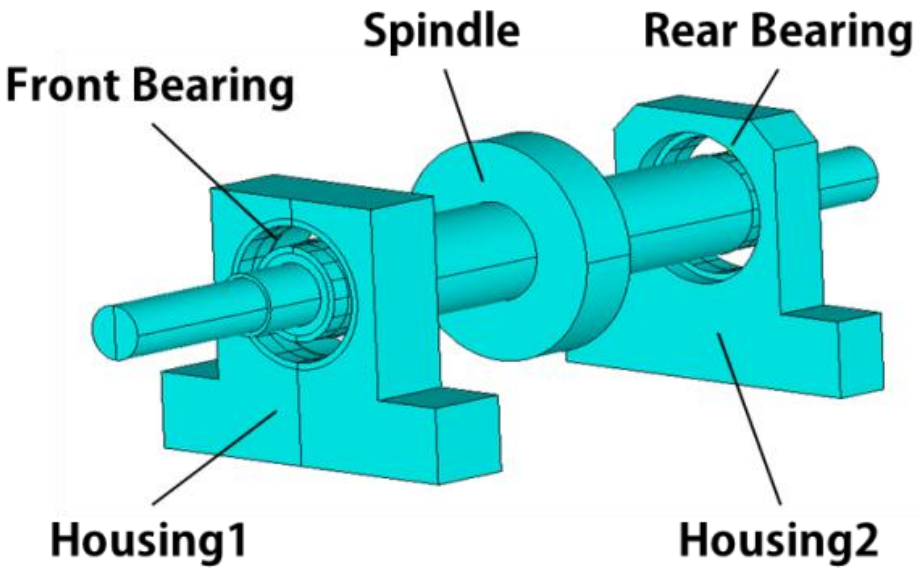

Fig. 4-2. 3D CAD model of the rotating unit.

We carried out a static analysis using SOLID227 elements with 10 nodes for the structural–thermal coupled analysis. We used stiffness and damping Matrix27 elements as spring elements. To apply the spring elements, we drew lines between the inner and outer races of bearing; 16 lines were used for each bearing, and meshed using a line mesh, as shown in Fig. 4-3. For the remainder of the volume, we used automatic meshing, and the same number and position of nodes as in the thermal analysis, for a total of 41,870 nodes and 28,268 elements. Using the real constant option, the stiffness values were distributed among the spring elements to match the technical data from the bearing manufacturer. The bottom parts of the housing were fixed, and a static analysis was carried out.

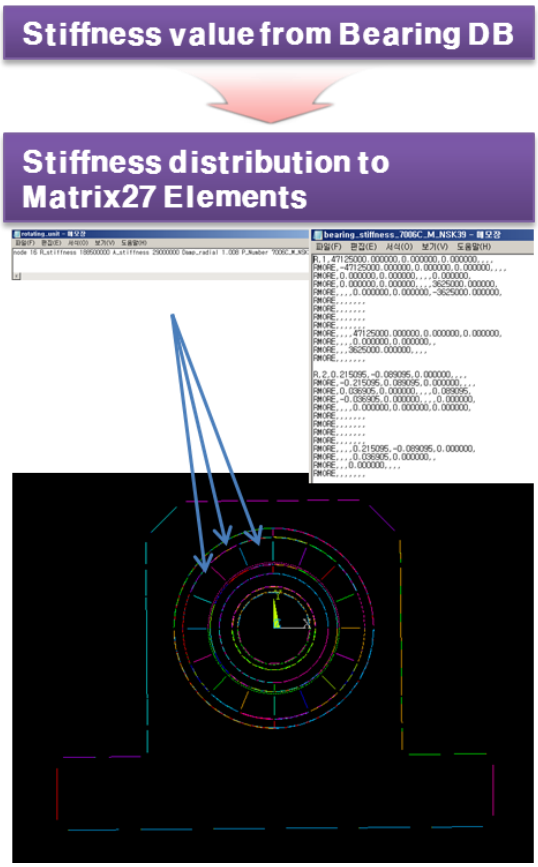

Fig. 4-3. Stiffness distribution used in the simulation.

Figures 4-4 to 4-6 show simulated temperature distributions for NSK7006C bearings with preloads of 150 N, 225 N, and 300 N. As expected, temperature increased when the magnitude of preload increased. Figures 4-7 to 4-9 show the result of the thermo-mechanical analysis of the same rotating units, using the temperature distributions shown in Figs. 4-4 to 4-6.

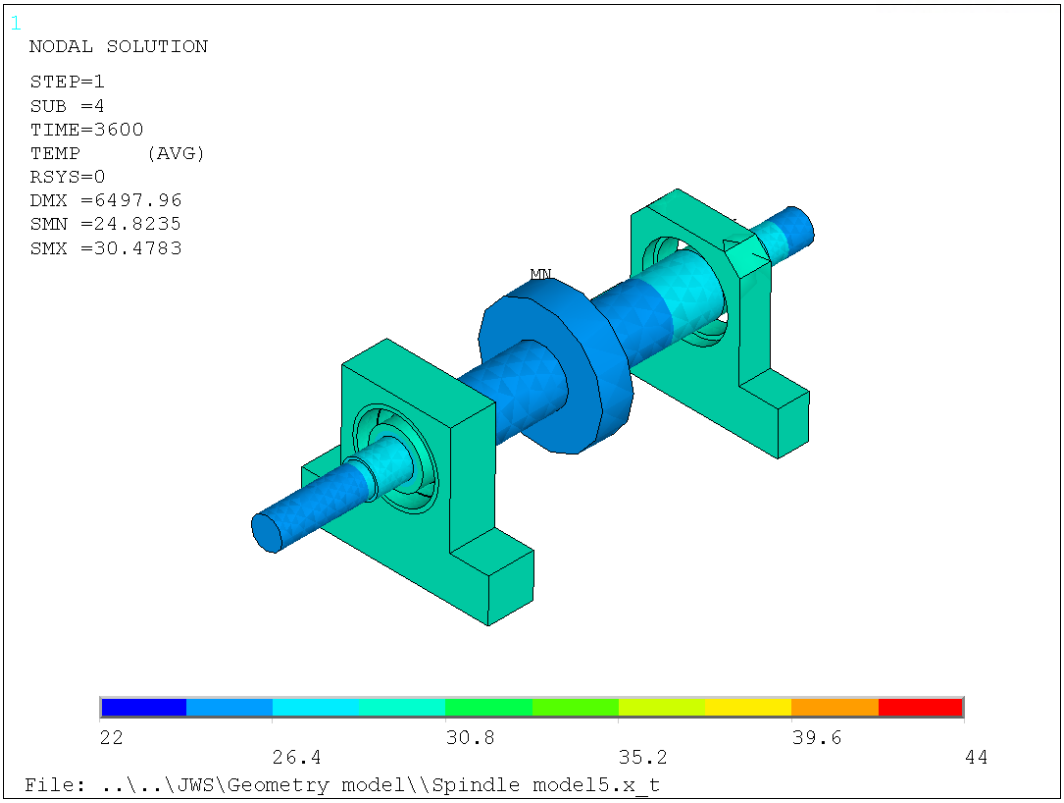

Fig. 4-4. Temperature distribution of rotating unit with a preload of 150 N.

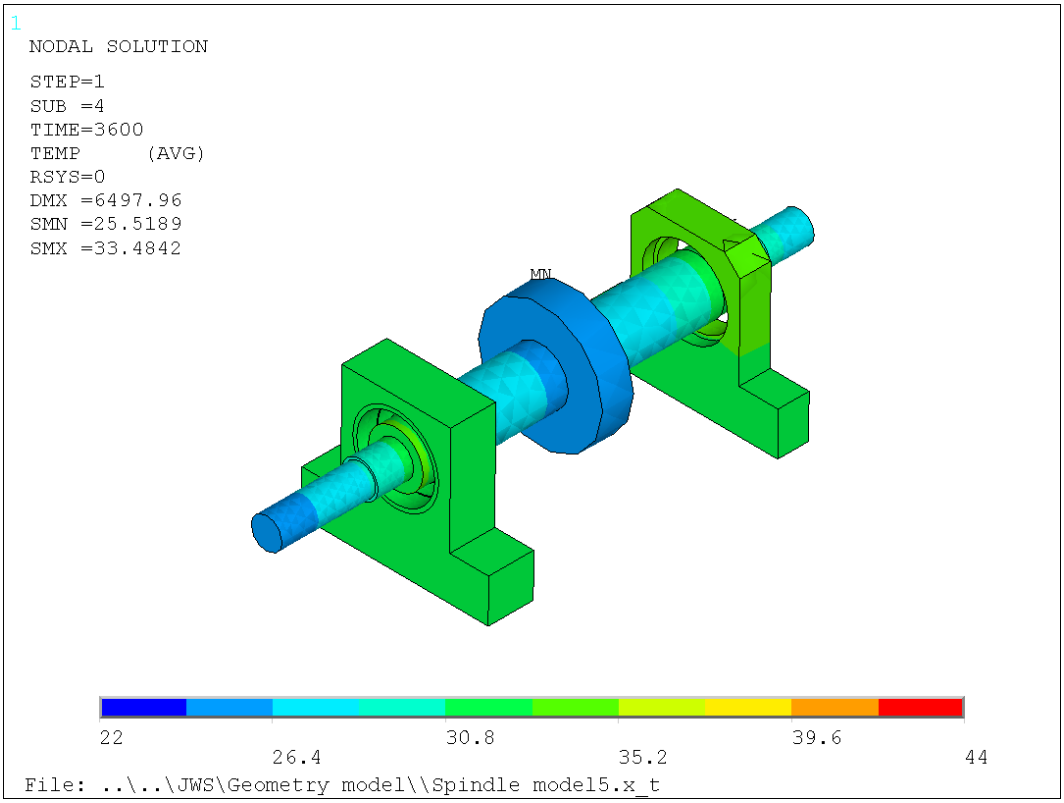

Fig. 4-5. Temperature distribution of rotating unit with a preload of 225 N.

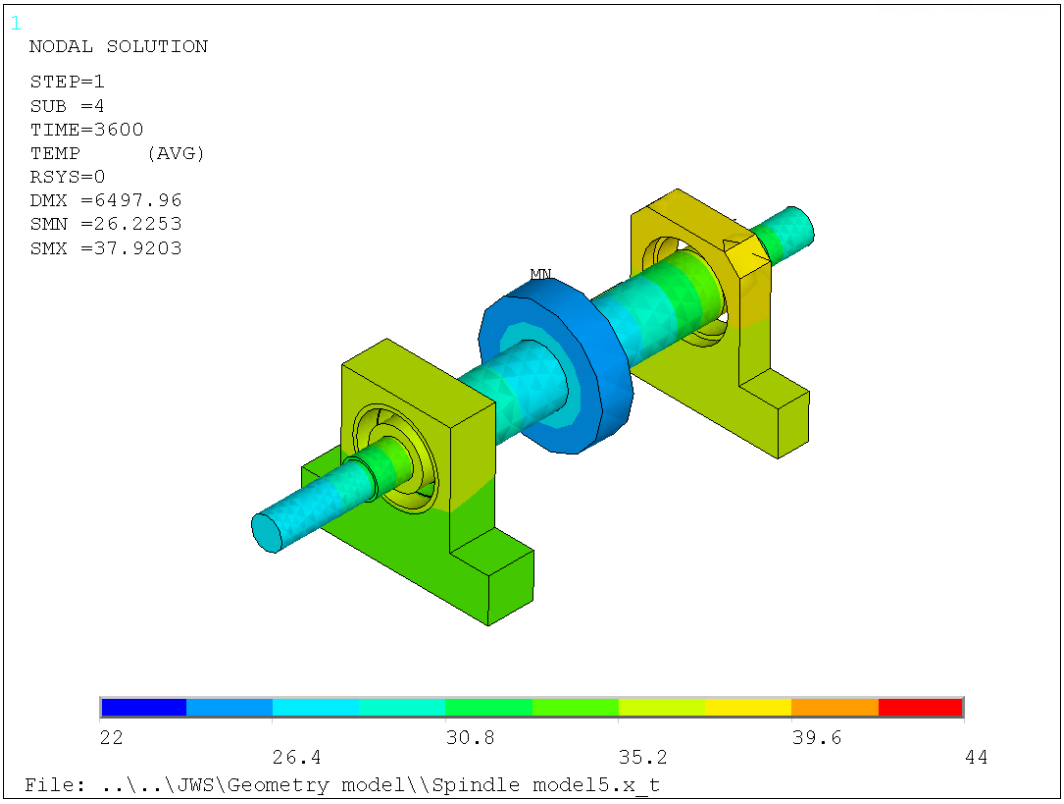

Fig. 4-6. Temperature distribution of rotating unit with a preload of 300 N.

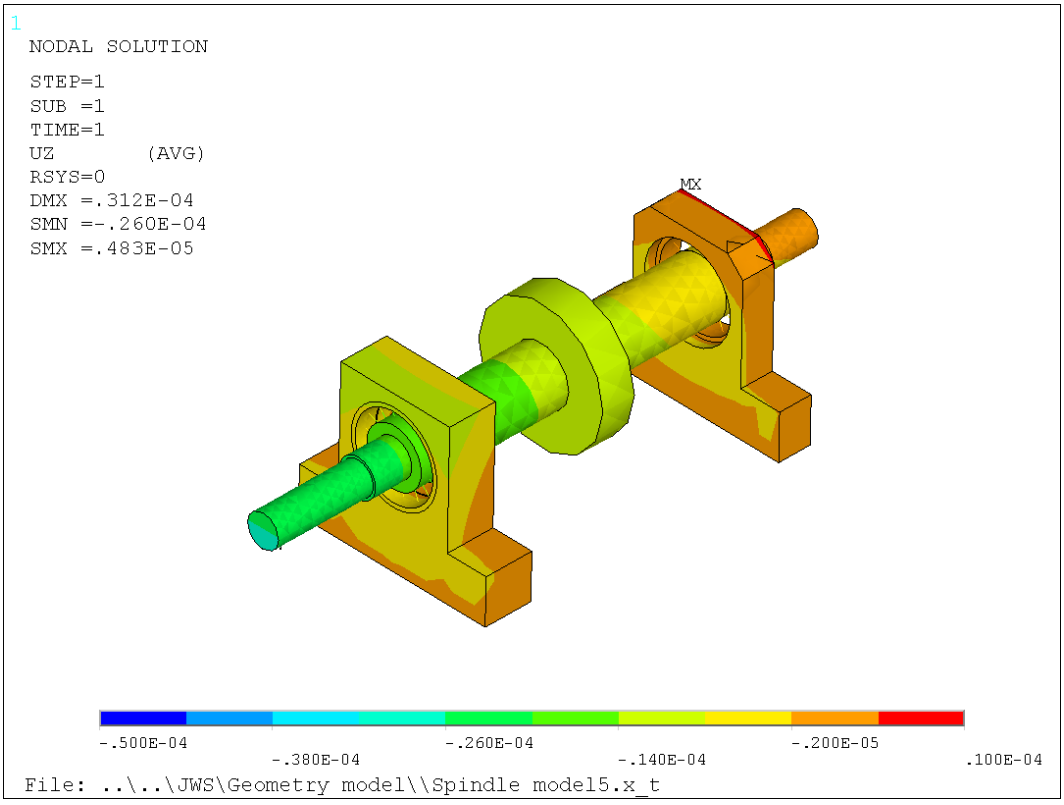

Fig. 4-7. Thermal deformation of the rotating unit with preload of 150 N.

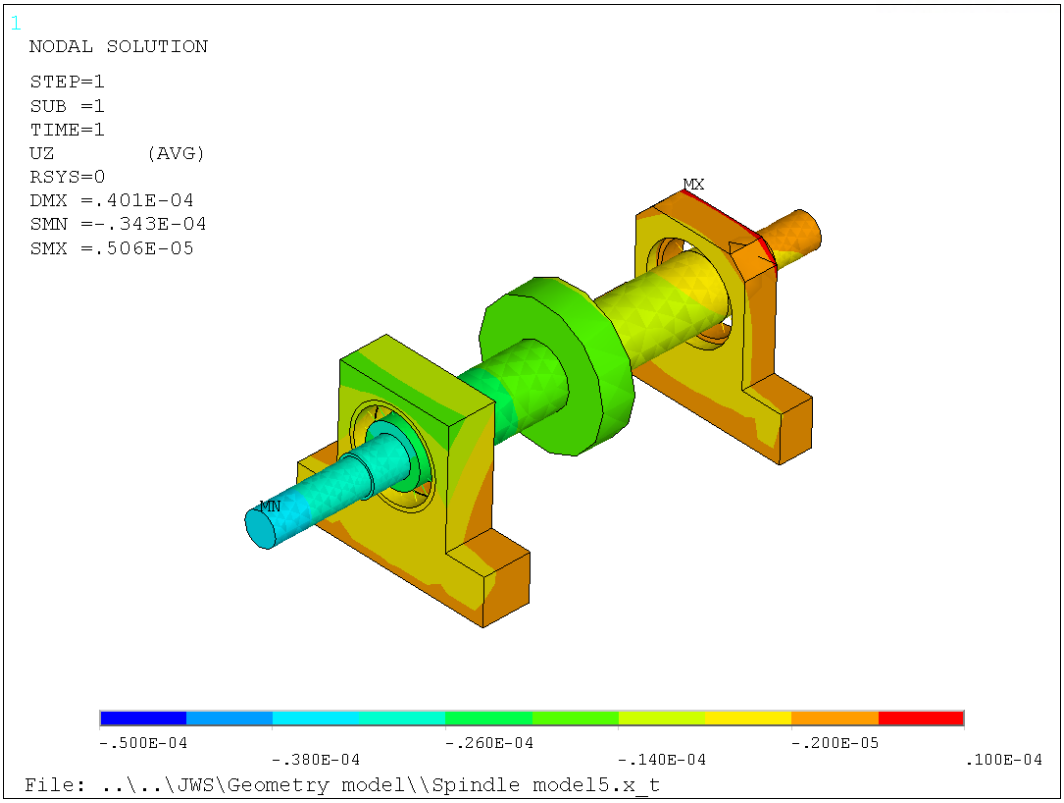

Fig. 4-8. Thermal deformation of the rotating unit with preload of 225 N.

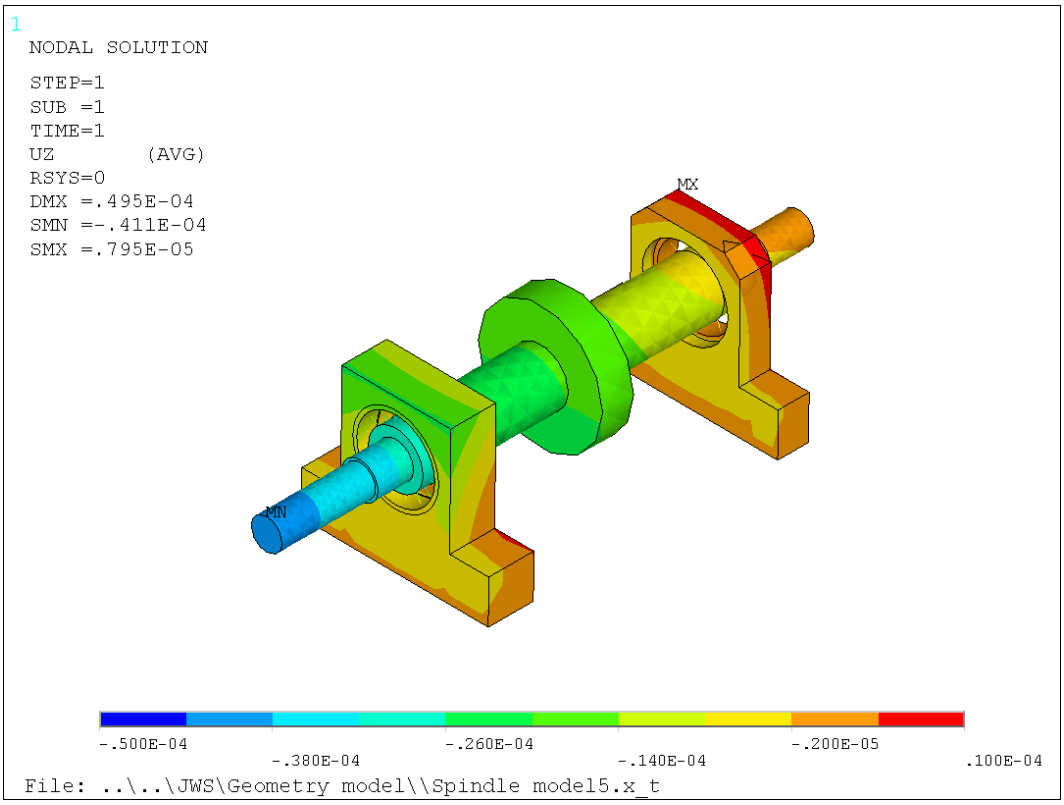

Fig. 4-9. Thermal deformation of the rotating unit with preload of 300 N.

4.2 Experimental setup of the rotating unit

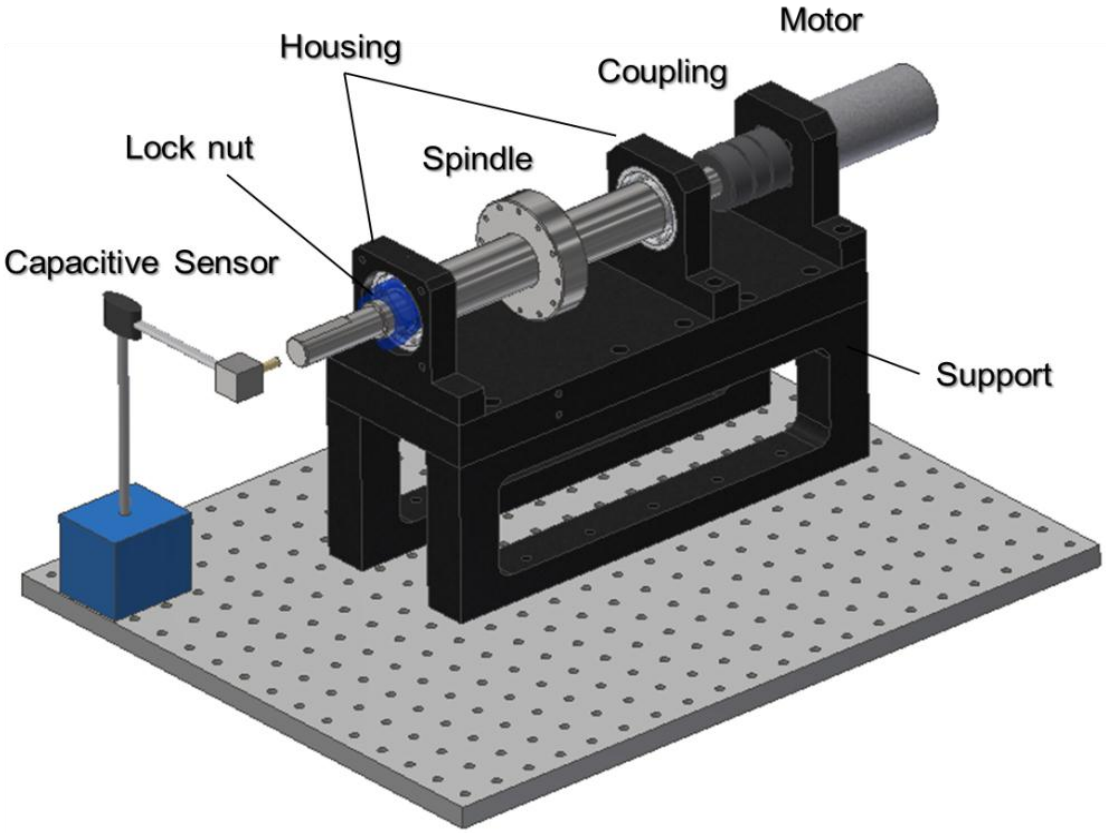

Fig. 4-10. Experimental setup used to characterize the rotating unit.

Figure 4-10 shows the experimental spindle system used to investigate the thermo-mechanical properties of the rotating unit. We used a GGM Ltd. motor with a brake power of 40 W and a maximum speed of 3000 rpm. We arranged two bearings in an O configuration: these were 7006C super-precision angular contact bearings manufactured by NSK and Nachi. We used the position preload method to provide loads to the bearings using a locking nut, and fixed the spindle system on a vibration isolation table. Lubrication is one of the most significant factors affecting the thermal properties of bearings, so we used base oil. Thermocouples were located on the outer bearing ring, and connected via a hole in the housing unit. We used a gap conductance sensor (Nanotex Ltd.) to measure the thermal deformation of the spindle, and recorded the signals from the gap conductance sensor and thermocouples using the Labview module DAQ 9172. We analyzed the thermal deformation of the spindle system was analyzed for three different types of bearing, each with three applied preloads. We repeated each experiment five times, and averaged these data for use in analyses.

4.3 Results and analysis of simulation and experiment

Figure 4-11 shows the simulated and measured time dependence of the temperature of the outer race of the NSK7006C bearing with a preload of 300 N. The steady-state temperature differed slightly, but the dependence on time was similar. Table 4-1 lists the results of FEM simulations and experiments for the NSK7006C, NSK7006A5, and Nachi7006C bearings for the preloads. Figures 4-12 and 4-13 compare the temperature and deformation. The error between the experimental results and the simulations increased as the preload increased. With the Nachi7006C bearing, the largest error occurred with a preload of 150 N. The average error in the datasets for the thermal analysis was 9.6%. The average error for the thermal deformation result was 9.5%. Such errors are inevitable because the simulation model was transformed to a simplified geometry, the experiments were carried out without using a thermostatic chamber, and centrifugal effects were not considered.

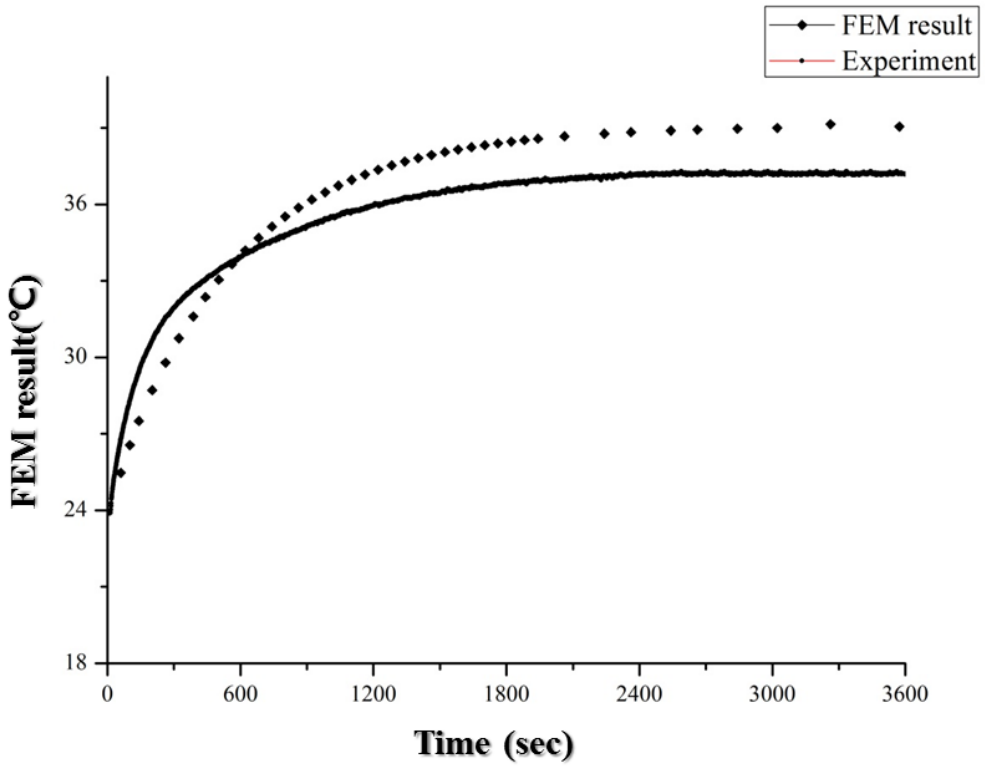

Fig. 4-11. Time dependence of the simulated and measured temperature of the outer race of the NSK7006C bearing.

Table 4-1. Temperature and deformation of the rotating unit. The temperature difference is the difference between the initial and final temperatures. The thermal deformation is the change in distance between the spindle tip compared with the starting location. Here. error corresponds to the difference between the simulated and measured data.

	Temperature difference [℃]			Thermal deformation [μm]		
	Simulation	Measurement	Error [%]	Simulation	Measurement	Error [%]
			NSK7006C			
150N	5.2	5.44	4.6	17.1	16	6.4
225N	8.74	8.56	2	32.5	30	7.7
300N	13.06	12.02	7.9	38.6	33	14.3
			NSK7006A5			
150N	5.6	5.89	5.2	24.4	20	18
225N	9.07	8.72	3.8	34.3	34	0.8
300N	12.6	10.47	16.9	41.4	45	8.7
			Nachi7006C			
150N	5.17	6.18	19.5	25.7	22	14.4
225N	8.3	9.87	19	33.6	31	7.1
300N	12.13	11.27	7.1	40.1	37	7.7

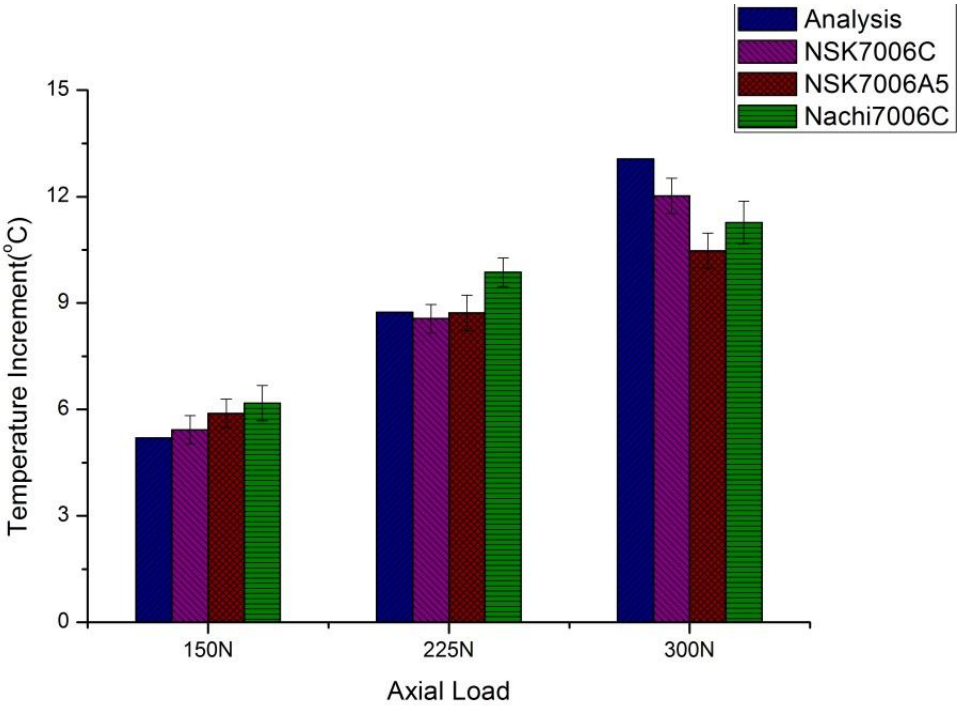

Fig. 4-12. Simulated and measured time dependence of the temperature of the rotating unit.

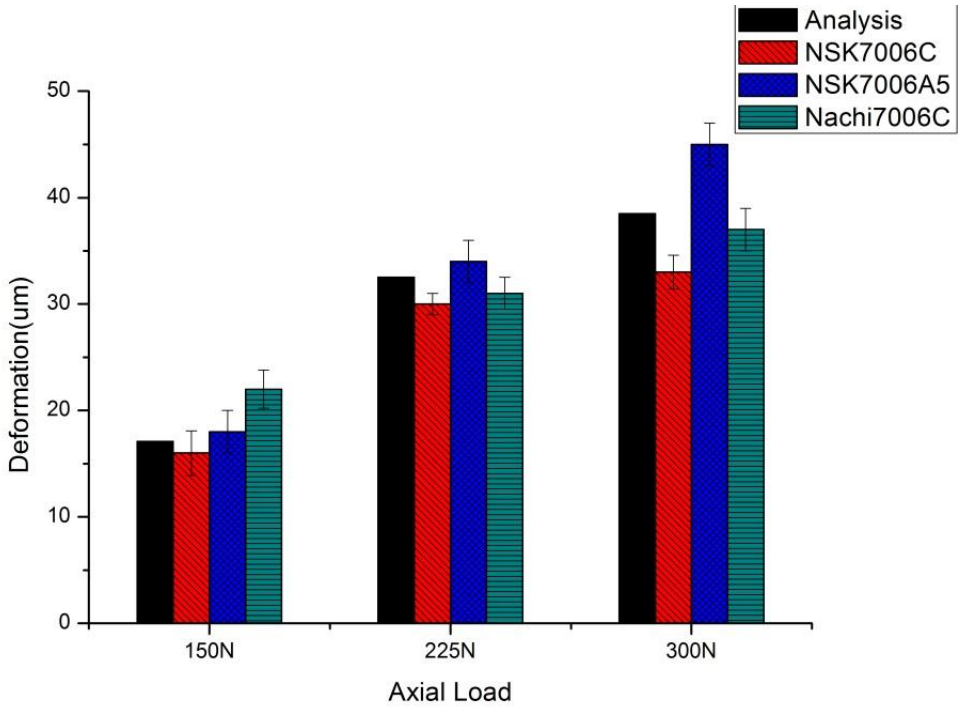

Fig. 4-13. Simulated and measured thermal deformation of the rotating unit.

4.4 Summary

In this chapter, we described the combination of the thermal, dynamic, and thermo-mechanical aspects of the simulation study, as well as the experimental verification. We discussed the details of the FEM simulation process, including thermal and static structural simulations. We applied the functions described in chapter 3 to account for the load, and applied the theoretical framework described in chapter 2. We used a 3D CAD model to analyze the geometry of the rotating unit, and imported it into the FEM simulation and meshed it using the automatic function. We carried out 1-hour transient thermal analyses, and transferred the resulting temperature information. We used Matrix 27 elements to describe the stiffness of bearing, and conducted a static structural analysis of the thermal deformation. We measured the temperature of the outer race of the bearing using thermocouples, measured the spindle deformation using a gap conductance sensor to verify the simulated data.

5. CONCLUSIONS AND RECOMMENDATIONS

5.1 Summary

We developed a method to simulate the thermo-mechanical behavior of a rotating unit using FEM. We used the software package ANSYS, and implemented its functions to describe the coupled thermo-mechanical behavior of the rotating unit. Chapter 2 presented the main factors affecting the behavior of the rotating unit. Angular contact bearings are the main source of heat in machine tools: we applied general equations for heat generation, including the effects of rotation on convection heat transfer. In chapter 3, we presented a thermo-mechanical model of the angular contact bearing. We developed a simplified bearing model and applied the heat transfer characteristics of the angular contact bearings to the simulation using a contact function and TCC; we parametrized TCC by comparing the simulated and measured temperature distributions. In chapter 4, we presented a thermo-mechanical analysis of the rotating unit using the techniques discussed in chapter 3. Comparison of the simulated and measured data revealed that agreement was achieved to within 9.6% for the temperature distribution and 9.5% for the thermal deformation.

5.2 Contributions and Conclusions

The main contributions of this work are the development of an FEM model to describe the thermo-mechanical behavior of rotating units, using a simplified geometry yet retaining high accuracy. The method used here decreased the complexity of the FEM model compared with existing approaches, and consequently reduced computational costs.

The main contributions of Chapter 3 are:

- We developed a method to simplify the geometry of angular contact ball bearings, and applied this in an FEM analysis of the thermo-mechanical behavior.
- We described the stiffness of the coupling section of the angular contact ball bearing using Matrix27 elements.
- We used the close gap function in ANSYS to incorporate heat transfer in angular contact ball bearings.
- We extracted the thermal contact conductance values for various types of bearings, and determined the distribution proportion of heat generation with the TCC value for angular contact ball bearings.

The main contributions from Chapter 4 are:

- We developed a thermo-mechanical FEM model for several preload conditions using the bearing model described in chapter 3.
- We performed experiments with rotating units to verify the simulation results, which demonstrated the reliability of the thermo-mechanical simulation.

5.3 Future work

The simulation method described here includes a simplification process for the geometry of the bearings, together with the use of some empirical approaches to improve agreement with experimental results. A number of areas remain for future work. First, dynamic characteristics, such as gyroscopic effects and the centrifugal force on the spindle, should be considered to describe the behavior of spindle system in more detail. Second, we achieved the thermal contact conductance values for static conditions (see section 3.4), but obviously rotating conditions are of more interest. Third, because the lubrication conditions affect the thermal characteristics of the angular contact bearing, there is significant scope for further investigation of the effects of various lubricants and lubrication configurations.

REFERENCE

ABELE, E., ALTINTAS, Y. & BRECHER, C. 2010. Machine tool spindle units. *CIRP Annals - Manufacturing Technology,* 59**,** 781-802.

ALFARES, M. A. & ELSHARKAWY, A. A. 2003. Effects of axial preloading of angular contact ball bearings on the dynamics of a grinding machine spindle system. *Journal of Materials Processing Technology,* 136**,** 48-59.

BOSSMANNS, B. & TU, J. F. 1999. A thermal model for high speed motorized spindles. *International Journal of Machine Tools and Manufacture,* 39**,** 1345-1366.

BOSSMANNS, B. & TU, J. F. 2001. A Power Flow Model for High Speed Motorized Spindles—Heat Generation Characterization. *Journal of Manufacturing Science and Engineering,* 123**,** 494.

BRECHER, C., SPACHTHOLZ, G. & PAEPENM LLER, F. 2007. Developments for High Performance Machine Tool Spindles. *CIRP Annals - Manufacturing Technology,* 56**,** 395-399.

CAO, Y. & ALTINTAS, Y. 2004. A General Method for the Modeling of Spindle-Bearing Systems. *Journal of Mechanical Design,* 126**,** 1089.

CHAPMAN, J. J. 1995. Angular Contact Ball Bearing Dynamics, an Experimental and Theoretical Investigation. 30**,** 435-443.

CHEN, D., BONIS, M., ZHANG, F. & DONG, S. 2011. Thermal error of a hydrostatic spindle. *Precision Engineering,* 35**,** 512-520.

CHEN, J.-S. & CHEN, K.-W. 2005. Bearing load analysis and control of a motorized high speed spindle. *International Journal of Machine Tools and Manufacture,* 45**,** 1487-1493.

CHOI, J. K. & LEE, D. G. 1998. Thermal characteristics of the spindle bearing system with a gear located on the bearing span. *International Journal of Machine Tools & Manufacture,* 38**,** 1017-1030.

CLOUGH, D., FLETCHER, S., LONGSTAFF, A. P. & WILLOUGHBY, P. 2012. Thermal Analysis for Condition Monitoring of Machine Tool Spindles. *Journal of Physics: Conference Series,* 364**,** 012088.

CREIGHTON, E., HONEGGER, A., TULSIAN, A. & MUKHOPADHYAY, D. 2010. Analysis of thermal errors in a high-speed micro-milling spindle. *International Journal of Machine Tools and Manufacture,* 50**,** 386-393.

CREMERS, C. J., KREITH, F., CLARK, J. A., AMERICAN SOCIETY OF MECHANICAL ENGINEERS. HEAT TRANSFER DIVISION. COMMITTEE ON THEORY AND FUNDAMENTAL RESEARCH. & AMERICAN SOCIETY OF MECHANICAL ENGINEERS. COMMITTEE ON AIRCRAFT AND ASTRONAUTICAL HEAT

TRANSFER. 1971. *Environmental and geophysical heat transfer,* New York,, American Society of Mechanical Engineers.

DEPING LIU, H. Z., ZHENG TAO AND YUFENG SU 2011. Finite Element Analysis of High-Speed Motorized Spindle Based on ANSYS. *The Open Mechanical Engineering Journal,* 5.

HAITAO, Z., JIANGUO, Y. & JINHUA, S. 2007. Simulation of thermal behavior of a CNC machine tool spindle. *International Journal of Machine Tools and Manufacture,* 47**,** 1003-1010.

HARRIS, T. A. & KOTZALAS, M. N. 2007. *Rolling bearing analysis,* Boca Raton, FL, CRC/Taylor & Francis.

HOLKUP, T., CAO, H., KOL Ř, P., ALTINTAS, Y. & ZELEN , J. 2010. Thermo-mechanical model of spindles. *CIRP Annals - Manufacturing Technology,* 59**,** 365-368.

JIANG, S. & MAO, H. 2010. Investigation of variable optimum preload for a machine tool spindle. *International Journal of Machine Tools and Manufacture,* 50**,** 19-28.

JORGENSEN, B. R. & SHIN, Y. C. 1998. Dynamics of spindle-bearing systems at high speeds including cutting load effects. *Journal of Manufacturing Science and Engineering,* 120**,** 387-394.

KIM, H.-M., SEO, J.-W. & PARK, H.-W. 2012. Computational Modeling of the Bearing Coupling Section of Machine Tools. *Journal of the Korean Society of Precision Engineering,* 29**,** 1050-1055.

KIM, J.-J., JEONG, Y. H. & CHO, D.-W. 2004. Thermal behavior of a machine tool equipped with linear motors. *International Journal of Machine Tools and Manufacture,* 44**,** 749-758.

KIM, S. I. & CHO, J. W. 2007. Thermal characteristic analysis of a high-precision centerless grinding machine for machining ferrules. *International Journal of Precision Engineering and Manufacturing,* 8**,** 32-37.

KIM, S. M. & LEE, S. K. 2001. Prediction of thermo-elastic behavior in a spindle-bearing system considering bearing surroundings. *International Journal of Machine Tools & Manufacture,* 41**,** 809-831.

KO, T. J., GIM, T. W. & HA, J. Y. 2003. Particular behavior of spindle thermal deformation by thermal bending. *International Journal of Machine Tools & Manufacture,* 43**,** 17-23.

KOLAR, P., SULITKA, M. & JANOTA, M. 2010. Simulation of dynamic properties of a spindle and tool system coupled with a machine tool frame. *The International Journal of Advanced Manufacturing Technology,* 54**,** 11-20.

KREITH, F., MANGLIK, R. M., BOHN, M. & TIWARI, S. 2011. *Principles of heat transfer,* Stamford, Conn., Cengage Learning.

KRULEWICH, D. A. 1998. Temperature integration model and measurement point selection for thermally induced machine tool errors. *Mechatronics,* 8**,** 395-412.

LEI, C. L., RUI, Z. Y., ZHOU, B. C. & FANG, J. F. 2013. A Study of High-Speed Angular Contact

Ball Bearing Thermo-Mechanical Coupling Characteristics. *Applied Mechanics and Materials,* 397-400**,** 131-134.

LI, H. & SHIN, Y. C. 2004a. Analysis of bearing configuration effects on high speed spindles using an integrated dynamic thermo-mechanical spindle model. *International Journal of Machine Tools and Manufacture,* 44**,** 347-364.

LI, H. & SHIN, Y. C. 2004b. Integrated Dynamic Thermo-Mechanical Modeling of High Speed Spindles, Part 1: Model Development. *Journal of Manufacturing Science and Engineering,* 126**,** 148.

LI, H. & SHIN, Y. C. 2004c. Integrated Dynamic Thermo-Mechanical Modeling of High Speed Spindles, Part 2: Solution Procedure and Validations. *Journal of Manufacturing Science and Engineering,* 126**,** 159.

LIN, C.-W., TU, J. F. & KAMMAN, J. 2003. An integrated thermo-mechanical-dynamic model to characterize motorized machine tool spindles during very high speed rotation. *International Journal of Machine Tools and Manufacture,* 43**,** 1035-1050.

LIN, Z.-C. & CHANG, J.-S. 2006. The building of spindle thermal displacement model of high speed machine center. *The International Journal of Advanced Manufacturing Technology,* 34**,** 556-566.

MIAN, N. S., FLETCHER, S., LONGSTAFF, A. P. & MYERS, A. 2011. Efficient thermal error prediction in a machine tool using finite element analysis. *Measurement Science & Technology,* 22.

MIN, X., SHUYUN, J. & YING, C. 2007. An improved thermal model for machine tool bearings. *International Journal of Machine Tools and Manufacture,* 47**,** 53-62.

MIZUTA, K., INOUE, T., TAKAHASHI, Y., HUANG, S., UEDA, K. & OMOKAWA, H. 2003. Heat transfer characteristics between inner and outer rings of an angular ball bearing. *Heat Transfer?Asian Research,* 32**,** 42-57.

NELSON, H. 1980. A finite rotating shaft element using Timoshenko beam theory. *Journal of Mechanical Design,* 102**,** 793-803.

PINEL, S. I., SIGNER, H. R. & ZARETSKY, E. V. 2001. Design and Operating Characteristics of High-Speed, Small-Bore Cylindrical-Roller Bearings. *Tribology Transactions,* 44**,** 70-78.

PRUVOT, F. C. & MOTTU, A. 1980. High Speed Bearings for Machine Tool Spindles. *CIRP Annals - Manufacturing Technology,* 29**,** 293-297.

RAI, J. K. & XIROUCHAKIS, P. 2008. FEM-based prediction of workpiece transient temperature distribution and deformations during milling. *The International Journal of Advanced Manufacturing Technology,* 42**,** 429-449.

RUHL, R. L. & BOOKER, J. 1972. A finite element model for distributed parameter turborotor systems. *Journal of Manufacturing Science and Engineering,* 94**,** 126-132.

SHUZI, Y. 1980. A study of the static stiffness of machine tool spindles. *International Journal of Machine Tools and Manufacture*, 21.

TERMAN, T. & BOLLINGER, J. 1965. Graphical method for finding optimum bearing span for overhung shafts. *Mach. Des,* 37**,** 159-162.

WANG, P., LEI, C. L., ZHOU, B. C. & ZHAO, W. P. 2013. Finite Element Analysis for Thermal Characteristics of High Speed Angular Contact Ball Bearing. *Applied Mechanics and Materials,* 397-400**,** 126-130.

ZAHEDI, A. & MOVAHHEDY, M. R. 2012. Thermo-mechanical modeling of high speed spindles. *Scientia Iranica,* 19**,** 282-293.

ZHANG, H., YANG, J., ZHANG, Y., SHEN, J. & WANG, C. 2010. Measurement and compensation for volumetric positioning errors of CNC machine tools considering thermal effect. *The International Journal of Advanced Manufacturing Technology,* 55**,** 275-283.

ACKNOWLEDGEMENTS

First and Foremost I offer my sincerest gratitude to my advisor, Prof. Hyung Wook Park, who has supported me thoughout my thesis with his patience and knowledge. I attribute the level of my Master's degree to his encouragement and effort and without him this thesis, too, would not have been completed or written.

I also wish to thank Prof. Young-Bin Park and Jaeseon Lee for being my thesis committee and for their friendly guide.

Thanks also to all members of Multi-scale Hybrid Manufacturing Lab , Dr. Deka, Dr. Ravi, Kyongil Kong, Eunju Park, Dong Min Kim, Jisu Kim, Ineon Lee and Do Young Kim, for providing a good atmosphere for study. I am grateful to Hyun Myung Kim for his help to my research in various ways.

Finally, I thank my parents for supporting me throughout all my studies at university